miR155 Enhances Autophagy by Reducing MBD5 and METTL3 in Human Liver Cancer Stem Cells

Yanan Lu
Tongji University
Yingjie Chen
Tongji University
Xiaoru Xin
Tongji University
Shuting Song
Tongji University
Xiaoxue Jiang
Tongji University
Sijie Xie
Tongji University
Liyan Wang
Tongji University
Dongdong Lu (ludongdong@tongji.edu.cn)
Tongji University https://orcid.org/0000-0002-7417-4172

Research

Keywords: miR-155, liver cancer stem cell, epigenetic modification, autophagy, cell cycle proteins, H-Ras

Posted Date: September 23rd, 2020

DOI: https://doi.org/10.21203/rs.3.rs-80157/v1

Abstract

Background: miR-155 is a widely reported carcinogenic miRNA, with up-regulated expression in a variety of human cancers.

Methods: Liver cancer stem cells were isolated from Huh7 cells; gene infection, RT-PCR, Western blotting and tumorigenesis test *in vitro* and *in vivo* were performed to analyze the signaling pathway.

Results: we demonstrate that miR-155 inhibits the expression of MBD5 and METTL3 , reducing the expression of DNMT1. In particular, miR155 inhibits the interaction between MBD5 and DNMT1, thereby inhibiting the binding capacity among MBD5, DNMT1 and IGFII (H19 ICR, IGFII DMR, IGFII Enhancer) DNA, inhibiting IGFII DNA methylation modification. Importantly, miR-155 promotes the formation of DNA loops in the IGFII DNA region (H19 ICR-IGFII Enhancer, IGFII DMR-IGFII Enhancer). Therefore, miR155 promotes the binding ability of H19-pre miR675 to histone methyltransferases SUV39h2 dependent on the H19 ICR-IGFII enhancer DNA loop and enhances the methylation modification of histone H3 on the ninth lysine . Then, the binding ability of RNA polII to P300 was enhanced by the formation of H3K9me2-RNA polII-P300 complex. Furthermore, miR155 promotes the binding ability of the RNA PolII-P300 complex to the IGFII promoter dependent on the IGFII DMR-IGFII enhancer DNA loop and promotes the expression of IGFII. Further research shows that miR155 promotes the binding of IGFII to stemness factors and the loading of stemness factors into the promoter region of HGF, which promotes the expression of hepatocyte growth factor HGF. In particular, miR155 promotes the expression of albumin gene (ALB) via HGF-c-MET, and then promotes the Sirt1 expression through ALB. Strikingly, miR155 promotes the autophagy dependent on acetylase Sirt1,including that miR155 promotes LC3 activation dependent on acetylase sirt1 and enhances binding capacity of LC3 to TP53INP2 / DOR, ATG4, ATG3 and ATG7, and the binding ability of the interaction between ATG5, ATG12, ATG6L1, ATG9. More meaningfully, miR155 enhances the ability of H-Ras to bind to the autophagosomes Beclin1, vps34, vps5, Uvrage, bif1, Lamp1, Lamp2, Lamp3, Rubicon, Rab24 dependent on autophagy, thereby enhancing the expression of H-Ras. Furthermore, miR155 enhances the expression of pRaf1, pMEK1 / 2, pERK1 / 2, pElK, pJak, Jun, pAKT, pmTOR, P70S6K, 4E-BP1, SGK1, C-myc dependent on H-Ras.Finally, miR-155 promotes the malignant growth of human liver cancer stem cells mediated by H-Ras.

Conclusions: these results provide a valuable theoretical basis for therapeutic targets of liver cancer based on miR-155.

Introduction

miR-155 is also a widely reported carcinogenic miRNA, with up-regulated expression in a variety of human cancers (1). Moreover, miR-155 modulates hepatic stellate cell proliferation(2) and exosome mediated miR-155 delivery confers cisplatin chemoresistance(3). Furthemore, miR-155 inhibits apoptosis(4) and PD-L1 expression(5). In particular, miR-155 promotes glioma progression(6) and the inhibition of miR-155 rejuvenates aged mesenchymal stem cells(7). So far, miR-155 has played a role in

the development of human liver cancer. The role is not yet clear, therefore, in-depth clarification of the molecular mechanism of miR-155 in the development of liver cancer is of great significance for the treatment of liver cancer.

Autophagy is a basic cellular process in eukaryotes and is essential for responding to and adapting to environmental changes. Cellular autophagy is mainly divided into three forms: microautophagy (Microautophagy), macroautophagy (Macroautophagy) and chaperone-mediated autophagy (CMA)(8). The ULK1 complex (ULK1, FIP200, ATG13 and ATG101) is assembled to initiate autophagosome formation(9). ATG16L1 complexes (ATG16L1, ATG5 and ATG12) are formed by ubiquitin-like coupling reaction(10) .Autophagy can be selectively degraded by autophagy receptors, including p62 (SQSTM1) that can bind cytoplasmic substrates (11) and NDP52(12). Methyl-CpG binding domain protein 5 (MBD5) is a member of the MBD protein family, which can selectively recognize methylated DNA and bind to methylated CpG(13). After MBD5 knocked down, the mTOR signaling pathway was also changed (14). Methyltransferase 3 (METTL3) is a major RNA N6-adenosyl methyltransferase that can participate in all stages of the RNA life cycle, including pre-mRNA splicing(15), 3’-end processing(16), nuclear export (17), translation regulation(18), and miRNA processing(19).DNA methyltransferase 1 (DNMT1) is a key enzyme that mediates DNA methylation and plays a key role in maintaining DNA methylation(20). Studies have indicated that DNMT1 is highly upregulated in tumor stem cells and is necessary to maintain the state of tumor stem cells(21).Insulin-like growth factor II (IGFII) is a pleiotropic hormone that can act as an autocrine, paracrine, and endocrine factor(22).Hepatocyte growth factor receptor MET interacts with its specific ligand HGF through the extracellular domain to form a MET-HGF dimer, thereby bringing the intracellular tyrosine kinase domains closer to each other(23), thereby promoting downstream signaling pathways, such as PI3K/AKT pathway and Wnt pathway (24). Ras protein is an important part of the intracellular signal pathway, which can regulate various basic cell activities, such as cell proliferation, apoptosis, differentiation and aging(25)

In this study, we demonstrate that miR-155 can promote the growth ability of liver cancer stem cells and the malignant transformation of hepatocyte-like cells. miR-155 targets MBD5 and METTL3 and reduces the three of IGF II DNA methylation binding regions (H19 ICR, IGFII DMR, IGFII Enhancer) methylation modification, promoting the expression of IGFII and Sirt1 and the occurrence of cell autophagy. It promotes the expression of oncogene H-Ras in human liver cancer stem cells. Moreover, the study indicates that H-Ras detemies s the cancerous function of miR-155.

Materials And Methods

Cell Lines Huh7 and hLCSCs were were maintained in Dulbecco’s modified Eagle medium(Gibco BRL Life Technologies) supplemented with 10% heat-inactivated fetal bovine serum (sigma) in a humidified atmosphere of 5% CO_2 incubator at 37ºC.

CD133+/CD44 + Huh7 cells sorting CD133/CD44 MicroBead Kits were purchased from Miltenyi technic(Boston,USA) and MACS® Technology operation according to and the operation according to the

manufacturer.

microRNA Detection Total RNA was isolated from cultured cells using Trizol (Invitrogen) according to the manufacturer's protocol or total RNA. RT-PCR-based detection of mature miR-155 and U6snRNA was achieved with a *mir*Vana miRNA Detection Kit and gene-specific primers (Ambion).

Western Blotting proteins were separated on a 10% sodium dodecyl sulfate-polyacrylamide gel electrophoresis (SDS-PAGE)and transferred onto a nitrocellulose membranes (Invitrogen, Carlsbad, CA,USA), and then blocked in 10% dry milk-TBST (20 mM Tris-HCl [PH 7.6], 127 mM NaCl, 0.1% Tween 20) for 1 h at 37 °C. Following three washes in Tris-HCl pH 7.5 with 0.1% Tween 20, the blots were incubated with 0.2 μg/ml of antibody (appropriate dilution) overnight at 4 °C. Following three washes, membranes were then incubated with secondary antibody for 60 min at 37 °C. Signals were visualized by enhanced chemiluminescence plus kit(GE Healthcare).

RNA Immunoprecipitation(RIP) Ribonucleoprotein particle-enriched lysates were incubated with protein G/A-plus agarose beads (Santa Cruz, Biotechnology,Inc.CA) together with antibody or normal rabbit IgG for 4 hours at 4 °C. Beads were subsequently washed four times with 50 mM TRIS/HCl, pH 7.0, 150 mM NaCl, 1 mM $MgCl_2$, and 0.05% NP-40, and twice after addition of 1M Urea. IPs were digested with proteinase K (55 °C; 30') and mRNAs were isolated and then RT-PCR was performed.

DNA pull down Cells were lysed by sonication in HKMG buffer (10 mM HEPES, PH7.9, 100 mM KCl, 5 mM $MgCl_2$, 100% glycerol, 1 mM DTT, and 0.5% NP40) containing protease and phosphatase inhibitors for the preparation of nuclear exact. Equal amount of cell nuclear extracts were precleared with Streptavidin-agarose Resin (Thermo) for 1 hours, and then were incubated with 1 μg biotinylated double-stranded-oligonucleotides and together with 10 μg poly(dI-dC) at 4 °C for 24 hours. DNA-bound proteins were collected with the incubation with streptavidin-agarose Resin for 1 hour with gently shaking to prevent precipitation in solution. Following 5 washings of the resin bound complex with 0.5-1.0 ml of binding buffer, the samples were boiled and subjected to SDS-PAGE and Western blot analysis.

Super-RNA-EMSA Cells were washed and scraped in ice-cold PBS to prepare nuclei for electrophoretic gel mobility shift assay with the use of the gel shift assay system (Promega) modified according to the manufacturer's instructions.

Chromosome conformation capture (3C) assay Cells were treated with 1% formaldehyde. Nuclei were resuspended in 500 μl of 1.2 × restriction enzyme buffer at 37 °C for 1 h. 7.5 μl of 20% SDS was added, the mixture was incubated for 1 h, followed by addition of 50 μl of 20% Triton X-100, and then incubation for an additional 1 h. Samples were then incubated with 400 units of selected restriction enzyme at 37 °C overnight. After digestion, 40 μl of 20% SDS was added to the digested nuclei, and the mixture was incubated at 65 °C for 10 min. 6.125 ml of 1.15 × ligation buffer and 375 μl of 20% Triton X-100 was added, the mixture was incubated at 37 °C for 1 h, and then 2000 units of T4 DNA ligase was added at 16 °C for a 4-h incubation.Samples were then de-cross-linked at 65 °C overnight followed by phenol-

chloroform extraction and ethanol precipitation. PCR products were amplified with AccuPrime Tag High Fidelity DNA Polymerase (Invitrogen)

Colony formation ability assay. cells were plated in 10 cm dish and incubated in a humidified atmosphere of 5% CO_2 incubator at 37ºC for 10 days. For visualization, colonies were stained with 0. 5% Crystal Violet (sigma) in 50% methanol and 10% glacial acetic acid. Colonies were counted using a dissecting microscope by MacBiophotonics Image J.

Tumorigenesis test in vivo Four-weeks male athymic Balb/C mice were maintained in the Tongji animal facilities. Balb/C mice were injected at the armpit area subcutaneously with cells in 100 µl of phosphate buffered saline. The mice were observed over 4 weeks for tumor formation. The mice were then sacrificed and the tumors recovered. The wet weight of each tumor was determined for each mouse. A portion of each tumor was fixed in 4% paraformaldehyde and embedded in paraffin for histological examination and anti-PCNA immunohistochemical staining.

Results

miR-155 promotes growth of human liver malignant stem cells

To address the effect of miR-155 on the growth of human liver cancer stem cells, first, as shown in Figure **S1A**, liver cancer stem cells were isolated from Huh7 cells using CD133 / CD44 / CD24 / EpCAM microbeads. In hLCSCs cells, CD133, CD44, CD24 and EpCAM were all positively expressed (Figure **S1B-C**). The green Fluorescent protein Green was expressed in rLV-hLCSCs, rLV-miR-155-hLCSCs, rLV-Cas9-hLCSCs, and rLV-Cas9-miR-155-hLCSCs (Fig. 1A). miR-155 was overexpressed in the rLV-miR-155 group compared with the rLV group and knocked-out in the rLV-Cas9-miR-155 group compared to the rLV-Cas9 group (Fig. 1B-F**)**. The proliferation ability was significantly increased in the rLV-miR-155 group compared with the rLV group (24 hours: $P = 0.000781 < 0.01$; 48 hours: $P = 0.0030012 < 0.01$) and significantly reduced in the rLV-Cas9-miR-155 group compared with the rLV-Cas9 group (24 hours: $P = 0.0020703 <$ 0.0148 hours: $P = 0.0068213 < 0.01$) **(**Fig. 2A**).** The positive rate of BrdU was significantly increased in the rLV-miR-155 group compared with the rLV group (27.94 ± 4.09% vs 69.86 ± 7.58%, $P = 0.00739 < 0.01$) and significantly reduced in the rLV-Cas9-miR-155 group compared with the rLV-Cas9 group (33.72 ± 5.39% vs 9.79 ± 1.26%, $P = 0.00996 < 0.01$) **(**Fig. 2B**)**. The colony formation rate in the rLV-miR-155 group was significantly increased in the rLV-miR-155 group compared with the rLV group (39.03 ± 3.28% vs 69.34 ± 5.57%, $P = 0.0097526 < 0.01$) and significantly reduced in the rLV-Cas9-miR-155 group compared with the rLV-Cas9 group (41.10 ± 4.21% vs 14.15 ± 2.33%, $P = 0.0073424 < 0.01$) **(**Fig. 2**Ca & b).** The phere formation rate was significantly increased in the rLV-miR-155 group compared with the rLV group (19.45 ± 1.84% vs 45.82 ± 3.45%, $P = 0.005133 < 0.01$); and significantly reduced in the rLV-Cas9-miR-155 group compared with the rLV-Cas9 group (21.04 ± 2.86% vs 21.04 ± 2.86%, $P = 0.0066237 < 0.01$) **(**Fig. 2 **Da & b)**. Compared to the rLV group, the rLV-miR-155 group had a significantly reduced The wide of scratches at 24 hours was significantly decreased in the rLV-miR-155 group compared with the rLV group increased in

the rLV-Cas9-miR-155 group compared with the rLV-Cas9 group **(**Fig. 2**Ea & b)**. The average weight of transplanted tumors was significantly increased in the rLV-miR-155 group compared with the rLV group (0.79 ± 0.0762 g vs 1.58 ± 0.149 g, P = 0.00002697 < 0.01) decreased in the rLV-Cas9-miR-155 group compared with the rLV-Cas9 group(0.82 ± 0.052 g vs. 0.11167 ± 0.0194079 g, P = 0.00000059 < 0.01) (Fig. 2**Fa & b).** The average time of transplanted tumors was significantly reduced was significantly increased in the rLV-miR-155 group compared with the rLV group (9.5 ± 1.04 days vs 6.67 ± 0.186 days, P = 0.0050136 < 0.01) and increased in the rLV-Cas9-miR-155 group compared with the rLV-Cas9 group (10 ± 1.41 days vs 15.5 ± 2.66 days, P = 0.00513 < 0.01) **(**Fig. 2**Fc)**. The poorly differentiated cancer cells and fewer middle differentiated cells were significantly increased in the rLV-miR-155 group compared with the rLV group and decreased in the rLV-Cas9-miR-155 group compared with the rLV-Cas9 group (Fig. 2G). Compared with the rLV group, rLV- The positive rate of PCNA positive rate was significantly increased in the rLV-miR-155 group compared with the rLV group (30.24 ± 3.47% vs 50.36 ± 9.65%, P = 0.0001083 < 0.01) and reduced in the rLV-Cas9-miR-155 group compared with the rLV-Cas9 group (32.51 ± 6.86% vs 10.84 ± 2.604%, p = 0.00034238 < 0.01) **(**Fig. 2**Ha-d).** Ki67 positive rate was significantly increased in the rLV-miR-155 group compared with the rLV group (44.02 ± 5.81% vs 83.43 ± 6.59%, P = 0.00005068 < 0.01) and reduced in the rLV-Cas9-miR-155 group compared with the rLV-Cas9 group (47.91 ± 7.97% vs 23.07 ± 3,61%, p = 0.00005799 < 0.01) (Fig. 2**Ia & b**). Collectiely, these observations suggest that miR-155 promotes the growth of liver cancer stem cells *in vitro and in vivo.*

miR-155 targets Methyl-CpG-binding domain protein 5 (MBD5) and RNA Methyltransferase-Like Protein3 (METTL3)

Bioinformatics analysis using MirTarget scanning soft software, RNA22 software, miRanda, RNA hybrid, PicTar and BLAST tools showed that the mature sequence of miR-155-5p was combined with MBD5 mRNA 3'-uncoding region (UTR) (2932–2953) (Fig. 3A). The activity of pEZX-MT-MDB 5 3'-UTR-Luc was significantly reduced in the rLV-miR-155 group compared with the rLV group (76251.56 ± 11668.42 vs 9672.003 ± 1382.79, P = 0.00618 < 0.01). On the contrary, the activity of pEZX-MT-MDB 5 3'-UTR-Luc was significantly increased in the rLV-Cas9-miR-155 group compared with rLV-Cas9 group (86894.67 ± 15844.88 vs 199439.23 ± 23410.45, P = 0.0088076 < 0.01) (Fig. 3B). pEZX-MT-MDB5 3'-UTR (mutant)-Luc luciferase reporter gene activity was significantly not altered among the four groups (Fig. 3C). Although the levels of MBD5 transcription in the four groups of cells was significantly not changed (Fig. 3D). However, the translation level of MBD5 was significantly reduced in the rLV-miR-155 group compared with the rLV group and was significantly increased in the rLV-Cas9-miR-155 group compared to the rLV-Cas9 group (Fig. 3E). The mature sequence of miR-155-3p is combined with the METTL3 mRNA 3'-noncoding region (UTR) (1426–1447) through an 11-base complementary seed sequence (Fig. 3F). The pEZX-MT-METTL3 3'-UTR-Luc luciferase reporter gene activity was significantly reduced in the rLV-miR-155 group compared with the rLV group (122002.64 ± 11425.88 vs 17965.38 ± 2418.83, P = 0.0029251 < 0.01) and significantly increased in the rLV-Cas9-miR-155 group compared to the rLV-Cas9 group (159774.01 ± 24414.41 vs 886606.15 ± 96030.39, P = 0.0017402 < 0.01) (Fig. 3G). pEZX-MT-METTL3 3'-UTR (mutant) -Luc luciferase reporter gene activity was not significantly changed among the four groups (Fig. 3H).

Although the transcription level of METTL3 was significantly altered in the four groups (Fig. 3I). However, the translation level of METTL3 was significantly reduced in the rLV-miR-155 group compared to the rLV group and significantly increased in rLV-Cas9-miR-155 group compared to the rLV-Cas9 group (Fig. 3J). Collectively, these results suggest that miR-155 targets MBD5 and METTL3, and inhibits the expression of MBD5 and METTL3.

miR-155 reduced the expression of DNA methyltransferase DNMT1 and the interaction between MBD5 and DNMT1 in human liver cancer stem cells by inhibiting METTL3

Given that miR-155 inhibits the expression of METTL3, we will adress whether miR-155 reduces the mRNA methylation modification of DNA methyltransferase DNMT1 in human liver cancer stem cells by inhibiting METTL3. The binding of METTL3 to DNMT1 mRNA was significantly reduced in rLV-miR-155 group compared to the rLV group and significantly increased in rLV-Cas9-miR-155 group compared to rLV-Cas9 group (Fig. 4A**)**. The binding of METTL3 to DNMT1 mRNA probes was significantly reduced in rLV-miR-155 group compared to the rLV group and significantly increased in rLV-Cas9-miR-155 group compared to rLV-Cas9 group **(Fig. 4Ba & b)**.The methylation modification of DNMT1 mRNA was significantly reduced in rLV-miR-155 group compared to the rLV group and significantly increased in rLV-Cas9-miR-155 group compared to rLV-Cas9 group **(** Fig. 4C**)**.pEZX-MT-DNMT1 3'-UTR-Luc luciferase reporter gene activity was significantly reduced in rLV-miR-155 group compared to the rLV group (88456.89 ± 9928.304 vs 8756.12 ± 1905.79, P = 0.0022279 < 0.01) and significantly increased in rLV-Cas9-miR-155 group compared to rLV-Cas9 group (86132.303 ± 14771.81 vs 218093.41 ± 18504.61, P = 0.0072004 < 0.01) **(**Fig. 4D).The expression of DNMT1 was significantly reduced in rLV-miR-155 group compared to the rLV group and significantly increased in rLV-Cas9-miR-155 group compared to rLV-Cas9 group (Fig. 4E **& F)**. Compared with hLCSCs, a control stable cell line infected with rLV, the expression of DNMT1 was significantly reduced in rLV-miR-155 group compared to the rLV group. However, the expression of DNMT1 was significantly not altered in the rLV-miR-155 + rLV-METTL3 group (Fig. 4G **& H**). The binding of MBD5 to DNMT1 was significantly reduced in rLV-miR-155 group compared to the rLV group and significantly increased in rLV-Cas9-miR-155 group compared to rLV-Cas9 group **(**Fig. 4I). Collectively,these results suggest that miR-155 inhibits the expression ability of DNMT1 gene and the interaction between MBD5 and DNMT1 dependent on METTL3.

miR155 inhibits the binding ability between MBD5 or DNMT1 and IGFII DNA methylation binding region (H19 ICR, IGFII DMR, IGFII Enhancer)

Since miR-155 inhibits the interaction between MBD5 and DNMT1, it will be considered whether miR-155 inhibits the three DNA methylation binding sequences (H19 ICR, IGFII DMR, IGFII Enhancer) regions of IGFII in liver cancer stem cells.The interaction between MBD5 and H19 ICR probe was significantly reduced in the the rLV-miR-155 group compared with the rLV group and was significantly increased in the rLV-Cas9-miR-155 group compared with the rLV-Cas9 group (Fig. 5A).The interaction between MBD5 and the IGFII DMR probe was significantly reduced in the rLV-miR-155 group compared with the rLV group and significantly increased in the rLV-Cas9-miR-155 group compared with the rLV-Cas9 group (Fig. 5B). The

interaction between MBD5 and the IGFII Enhancer probe was significantly reduced in the rLV-miR-155 group compared with the rLV group and significantly increased in the rLV-Cas9-miR-155 group compared with the rLV-Cas9 group (Fig. 5C). The interaction between MBD5 and H19 ICR probe was significantly reduced in the rLV-miR-155 group compared with the rLV group and significantly increased in the rLV-Cas9-miR-155 group compared with the rLV-Cas9 group (Fig. 5D). The interaction between MBD5 and IGFII DMR probe was significantly reduced in the rLV-miR-155 group compared with the rLV group and significantly increased in the rLV-Cas9-miR-155 group compared with the rLV-Cas9 group (Fig. 5E). The interaction between MBD5 and IGFII Enhancer probe was significantly reduced in the rLV-miR-155 group compared with the rLV group and significantly increased in the rLV-Cas9-miR-155 group compared with the rLV-Cas9 group (Fig. 5F). The interaction between the three DNA methylation binding region (H19 ICR, IGFII DMR, IGFII Enhancer) and MBD5 was significantly reduced in the rLV-miR-155 group compared with the rLV group and significantly increased in the rLV-Cas9-miR-155 group compared with the rLV-Cas9 group (Fig. 5G).The interaction between DNMT1 and H19 ICR probe was significantly reduced in the rLV-miR-155 group compared with the rLV group and significantly increased in the rLV-Cas9-miR-155 group compared with the rLV-Cas9 group (Fig. 5H). The interaction between DNMT1 and IGFII DMR probe w was significantly reduced in the rLV-miR-155 group compared with the rLV group and significantly increased in the rLV-Cas9-miR-155 group compared with the rLV-Cas9 group (Fig. 5I). The interaction between DNMT1 and IGFII Enhancer probe was significantly reduced in the rLV-miR-155 group compared with the rLV group and significantly increased in the rLV-Cas9-miR-155 group compared with the rLV-Cas9 group (Fig. 5J). The interaction between DNMT1 and H19 ICR probe was significantly reduced in the rLV-miR-155 group compared with the rLV group and significantly increased in the rLV-Cas9-miR-155 group compared with the rLV-Cas9 group (Fig. 5K).The interaction between DNMT1 and IGFII DMR probe was significantly reduced in the rLV-miR-155 group compared with the rLV group and significantly increased in the rLV-Cas9-miR-155 group compared with the rLV-Cas9 group (Fig. 5L). The interaction between DNMT1 and IGFII Enhancer probe was significantly reduced in the rLV-miR-155 group compared with the rLV group and significantly increased in the rLV-Cas9-miR-155 group compared with the rLV-Cas9 group (Fig. 5M). The three DNA methylation binding region (H19 ICR, IGFII DMR, IGFII Enhancer) and DNMT1 was significantly reduced in the rLV-miR-155 group compared with the rLV group and significantly increased in the rLV-Cas9-miR-155 group compared with the rLV-Cas9 group (Fig. 5N). Collectively,these results suggest that miR-155 inhibits the binding ability of MBD5 or DNMT1 to the three DNA methylation binding sequences (H19 ICR, IGFII DMR, IGFII Enhancer) in liver cancer stem cells.

miR155 inhibits DNA methylation modification of the three DNA regions on IGFII (H19 ICR, IGFII DMR, IGFII Enhancer)

To investigate the DNA methylation modification of three DNA sequences on IGFII (H19 ICR, IGFII DMR, IGFII Enhancer) ,the specific methylation PCR and Dot blot were used to detect this methylation modification in liver cancer stem cells. H19 ICR DNA methylation modification was significantly reduced in the rLV-miR-155 group compared with the rLV group and increased in the rLV-Cas9-miR-155 group compared with the rLV-Cas9 group (Fig. 6A). However, when DNMT1 was overexpressed or the DNA methylation inhibitor 5-Aza-2 was added in the cells, these effects were completely abolished (Fig. 6A).

The DNA methylation modification of IGFII DMR was significantly reduced in the rLV-miR-155 group compared with the rLV group and significantly increased in the rLV-Cas9-miR-155 group compared with the rLV-Cas9 group (Fig. 6B). The methylation modification of IGFII Enhancer DNA was significantly reduced in the rLV-miR-155 group compared with the rLV group and significantly increased in the rLV-Cas9-miR-155 group compared with the rLV-Cas9 group (Fig. 6B). The methylation modifications of H19 ICR, IGFII DMR, IGFII Enhancer DNA were significantly reduced in the rLV-miR-155 group compared with the rLV group and increased in the rLV-Cas9-miR-155 group compared with the rLV-Cas9 group (Fig. 6C&D). Collectively,these results suggest that miR-155 inhibits the methylation modification of three DNA methylation binding sequences (H19 ICR, IGFII DMR, IGFII Enhancer) on IGFII in liver cancer stem cells.

miR-155 promotes the formation of IGFII DNA loops (H19 ICR- IGFII Enhancer, IGFII DMR-IGFII Enhancer)

In order to investigate whether miR-155 affects the formation of DNA loops on the IGFII DNA region, we first analyzed the binding ability of CTCF to the three DNA methylation binding sequences (H19 ICR, IGFII DMR, IGFII Enhancer) in liver cancer stem cells. The interaction between CTCF and H19 ICR probe was significantly enhanced in the rLV-miR-155 group compared with the rLV group and significantly reduced in the rLV-Cas9-miR-155 group compared with the rLV-Cas9 group (Fig. 7A).The interaction between CTCF and IGFII DMR probe was significantly increased in the rLV-miR-155 group compared with the rLV group and significantly reduced in the rLV-Cas9-miR-155 group compared with the rLV-Cas9 group (Fig. 7B). The interaction between CTCF and IGFII Enhancer probe was significantly increased in the rLV-miR-155 group compared with the rLV group and significantly reduced in the rLV-Cas9-miR-155 group compared with the rLV-Cas9 group (Fig. 7C). The interaction between CTCF and H19 ICR probe was significantly increased in the rLV-miR-155 group compared with the rLV group and significantly reduced in the rLV-Cas9-miR-155 group compared with the rLV-Cas9 group (Fig. 7D). The interaction between CTCF and IGFII DMR probe was significantly increased in the rLV-miR-155 group compared with the rLV group and significantly reduced in the rLV-Cas9-miR-155 group compared with the rLV-Cas9 group (Fig. 7E). The interaction between CTCF and IGFII Enhancer probe was significantly increased in the rLV-miR-155 group compared with the rLV group and significantly reduced in the rLV-Cas9-miR-155 group compared with the rLV-Cas9 group (Fig. 7F). However, it was significantly altered in IGFII in rLV-miR-155 + rLV-MBD5 group, rLV-miR-155 + rLV-METTL2 group, rLV-miR-155 + rLV-DNMT1 group (Fig. 7G). The interaction between CTCF and the three DNA methylation binding sequences (H19 ICR, IGFII DMR, IGFII Enhancer) was significantly enhanced in the rLV-miR-155 group compared with the rLV group and significantly reduced in the rLV-Cas9-miR-155 group compared with the rLV-Cas9 group (Fig. 7H). However, it was significantly altered in rLV-miR-155 + rLV-DNMT1 group (Fig. 7I).The formation of H19 ICR-IGFII Enhancer DNA loops was increased significantly in the rLV-miR-155 group compared with the rLV group and significantly reduced in the rLV-Cas9-miR-155 group compared with the rLV-Cas9 group (Fig. 7J). The formation of IGFII-DMR-IGFII Enhancer DNA loops was significantly increased in the rLV-miR-155 group compared with the rLV group and significantly reduced in the rLV-Cas9-miR-155 group compared with the rLV-Cas9 group

(Fig. 7K). Collectively, these observations suggest that miR-155 enhances the formation of IGFII DNA loops (H19 ICR- IGFII Enhancer, IGFII DMR-IGFII Enhancer) in liver cancer stem cells.

miR155 enhances IGFII expression through the IGFII DNA loop

Given that miR155 reduces the methylation modification of H19 ICR DNA and promotes the formation of H19 ICR- IGFII Enhancer DNA loop, we will first analyze whether miR155 increases H19-pre miR675 (intragene gene, miR675 precursor is located in H19 Exons) transcription. The transcription level of H19-pre miR675 was significantly increased significantly in the rLV-miR-155 group compared with the rLV group and reduced in the rLV-Cas9-miR-155 group compared with the rLV-Cas9 group (Fig. 8A). The ability of H19-pre miR675 probe to bind to histone methyltransferase SUV39h2 was significantly increased significantly in the rLV-miR-155 group compared with the rLV group and reduced in the rLV-Cas9-miR-155 group compared with the rLV-Cas9 group (Fig. 8B). The binding ability of the H19-pre miR675 probe to histone methyltransferase SUV39h2 was significantly increased significantly in the rLV-miR-155 group compared with the rLV group and reduced in the rLV-Cas9-miR-155 group compared with the rLV-Cas9 group (Fig. 8C).The ability of H19-pre miR675 to bind to histone methyltransferases SUV39h2 or HistoneH3 was significantly increased significantly in the rLV-miR-155 group compared with the rLV group and reduced in the rLV-Cas9-miR-155 group compared with the rLV-Cas9 group (Fig. 8D). The binding ability of SUV39h2 to Histone H3 was significantly increased significantly in the rLV-miR-155 group compared with the rLV group and reduced in the rLV-Cas9-miR-155 group compared with the rLV-Cas9 group (Fig. 8E). However, it was significantly altered in the rLV-miR-155 + pGFP-V-RS-H19 group compared to rLV group (Fig. 8F). The H3K9me2 was significantly increased significantly in the rLV-miR-155 group compared with the rLV group and reduced in the rLV-Cas9-miR-155 group compared with the rLV-Cas9 group (Fig. 8G). However, it was significantly altered in the rLV-miR-155 + pGFP-V-RS-H19 group compared with the rLV group (Fig. 8H).The binding ability of H3K9me2 to RNApolII or P300 was significantly increased significantly in the rLV-miR-155 group compared with the rLV group and reduced in the rLV-Cas9-miR-155 group compared with the rLV-Cas9 group (Fig. 8I). However, it was significantly not altered in the rLV-miR-155 + pGFP-V-RS-H19 group compared to rLV group (Fig. 8J). Moreover, the binding ability of RNApolII to P300 was significantly altered in the rLV-miR-155 + rLV-JMJD2A (JMJD2A can inhibit H3K9me2) group compared with the rLV group (Fig. 8**KCa&b**). The ability of RNA PolII to enter the IGFII DMR-IGFII Enhancer loop was significantly increased significantly in the rLV-miR-155 group compared with the rLV group and reduced in the rLV-Cas9-miR-155 group compared with the rLV-Cas9 group (Fig. 8L). The ability of P300 to enter the IGFII DMR-IGFII Enhancer loop was significantly increased significantly in the rLV-miR-155 group compared with the rLV group and reduced in the rLV-Cas9-miR-155 group compared with the rLV-Cas9 group (Fig. 8M). However, The ability of RNA PolII to enter the IGFII DMR-IGFII Enhancer loop was significantly altered in the rLV-miR-155 + rLV-MBD5 and rLV-miR-155 + rLV-DNMT1 groups compared to rLV group (Fig. 8N). The ability of P300 to enter the IGFII DMR-IGFII Enhancer loop was significantly altered in the rLV-miR-155 + rLV-MBD5 and rLV-miR-155 + rLV-DNMT1 groups compared to rLV group (Fig. 8O). The binding ability of RNApolII or P300 to the IGFII promoter was

significantly increased significantly in the rLV-miR-155 group compared with the rLV group and reduced in the rLV-Cas9-miR-155 group compared with the rLV-Cas9 group (Fig. 8P). However, it ws not significantly altered in rLV-miR-155 + rLV-MBD5 and rLV-miR-155 + rLV-DNMT1 (Fig. 8Q). pEZX-MT- IGFII promoter -Luc activity was significantly increased significantly in the rLV-miR-155 group compared with the rLV group (352455.02 ± 37889.29 vs 2670666.56 ± 321009.37, P = 003626 < 0.01) and reduced in the rLV-Cas9-miR-155 group compared with the rLV-Cas9 group(340699.19 ± 51915.15 vs 73593.6 ± 15545.73, P = 0.0096644 < 0.01) (Fig. 8R). However, it was significantly altered in rLV-miR-155 + rLV-MBD5 group, rLV-miR-155 + rLV-DNMT1 group (253084.27 ± 16970.64 vs 221970.86 ± 27153.35, P = 0.1485 > 0.05; 253084.27 ± 16970.64 vs 247148.56 ± 26898.55, P = 0.4035 > 0.05) (Fig. 8S). The expression of IGFII was significantly increased (352455.02 ± 37889.29 vs 2670666.56 ± 321009.37, P = 003626 < 0.01) (Fig. 8T**&U)**. However, it was significantly not altered in rLV-miR-155 + rLV-MBD5 group and rLV-miR-155 + rLV-DNMT1 group compared to rLV group(Fig. 8V**&W**). Collectively,these results suggest that miR-155 enhances the expression of IGFII human liver cancer.

miR155 promotes the expression of hepatocyte growth factor HGF dependent on IGFII

Because Oct4, Nanog, Sox2, and C-myc are expressed in liver cancer stem cells, we will analyze the relationship between IGFII and these stem factors, thereby revealing whether miR155 plays a role by affecting these stem factors through IGFII in liver cancer stem cells. The binding ability of IGFII to Oct4, Nanog, Sox2, and C-myc was significantly increased in the rLV-miR-155 group compared with the rLV group and reduced in the rLV-Cas9-miR-155 group compared to the rLV-Cas9 group (Fig. 9A). The binding ability of Oct4, Nanog, Sox2, C-myc to HGF promoter was significantly increased in the rLV-miR-155 group compared with the rLV group and reduced in the rLV-Cas9-miR-155 group compared to the rLV-Cas9 group (Fig. 9B**)**. The binding ability of the HGF promoter probe to RNApolII was significantly increased in the rLV-miR-155 group compared with the rLV group and reduced in the rLV-Cas9-miR-155 group compared to the rLV-Cas9 group (Fig. 9C). The binding ability of RNApolII to the HGF promoter was significantly increased in the rLV-miR-155 group compared with the rLV group and reduced in the rLV-Cas9-miR-155 group compared to the rLV-Cas9 group (Fig. 9D). The HGF promoter luciferase reporter gene activity was significantly increased in the rLV-miR-155 group compared with the rLV group (244182.22 ± 26755.99, vs 991690.64 ± 96119.204, P = 0.00273075 < 0.01) and reduced in the rLV-Cas9-miR-155 group compared to the rLV-Cas9 group (234102.91 ± 36007.75 vs 47444.93 ± 8591.94, P = 0.007357251 < 0.01) (Fig. 9E). The expression of HGF was significantly increased in the rLV-miR-155 group compared with the rLV group and reduced in the rLV-Cas9-miR-155 group compared to the rLV-Cas9 group (Fig. 9F **& G**). The binding ability of Oct4, Nanog, Sox2, C-myc to HGF promoter was significantly enhanced in the rLV-miR-155 group compared with the rLV group. However, it wasn significantly altered in the rLV-miR-155 + pGFP-V-RS-IGFII group (Fig. 9H). The binding ability of the HGF promoter probe to RNApolII was significantly not increased in the rLV-miR-155 group compared with the rLV group. However, it wasn significantly altered in the rLV-miR-155 + pGFP-V-RS-IGFII group (Fig. 9I). The binding ability of RNApolII to the HGF promoter was significantly enhanced in the rLV-miR-155 group

compared with the rLV group. However, it was significantly not altered in the rLV-miR-155 + pGFP-V-RS-IGFII group (Fig. 9J). The HGF promoter luciferase reporter gene activity was significantly increased in the rLV-miR-155 group compared with the rLV group (145241.67 ± 10458.73 vs 772462.65 ± 100729.75, P = 0.0035029 < 0.01). However, it was significantly not altered in the rLV-miR-155 + pGFP-V-RS-IGFII group (145241.67 ± 10458.73vs 134490.03 ± 27214.11, P = 0.3080063 < 0.01) (Fig. 9K). The expression of HGF was significantly increased in the rLV-miR-155 group compared with the rLV group. However, it was significantly not altered in the rLV-miR-155 + pGFP-V-RS-IGFII group (Fig. 9L **& M**). Collectively, these results suggest that miR-155 enhances the expression of HGF dependent on IGFII t in human liver cancer stem cells.

miR155 promotes the expression of deacetylase Sirt1 dependent on HGF-MET

Because albumin ALB regulates the expression of many genes and miR155 promotes the expression of HGF in liver cancer stem cells, we will analyze whether miR155 affects the expression of ALB through HGF.The binding ability of HGF to c-MET was significantly increased in the rLV-miR-155 group compared with the rLV group and reduced in the rLV-Cas9-miR-155 group compared with the rLV-Cas9 group (Fig. 10A). The expression level of ALB was significantly increased in the rLV-miR-155 group compared with the rLV group and reduced in the rLV-Cas9-miR-155 group compared with the rLV-Cas9 group (Fig. 10B **& C**). The expression level of ALB was significantly increased in the rLV-miR-155 group compared with the rLV group. However, it was significantly not altered in the rLV-miR-155 + pGFP-V-RS-HGF group and rLV-miR-155 + pGFP-V-RS-c-MET group (Fig. 10 **& E**). The binding ability of Sirt1 promoter probe to ALB was significantly increased in the rLV-miR-155 group compared with the rLV group and reduced in the rLV-Cas9-miR-155 group compared with the rLV-Cas9 group **(**Fig. 10F). The ability of Sirt1 promoter to bind to ALB was significantly enhanced in the rLV-miR-155 group compared with the rLV group and reduced in the rLV-Cas9-miR-155 group compared with the rLV-Cas9 group (Fig. 10G).The Sirt1 promoter luciferase reporter gene activity was significantly increased in the rLV-miR-155 group compared with the rLV group (98765.34 ± 9580.63 vs 314101.303 ± 37418.49, P = 0.0065 < 0.01) and reduced in the rLV-Cas9-miR-155 group compared with the rLV-Cas9 group (81727.97 ± 15696.44 vs 15048.53 ± 2206.36, P = 0.0081916 < 0.01) (Fig. 10H). The binding ability of ALB to Sirt1 promoter was significantly enhanced in the rLV-miR-155 group compared with the rLV group. However, it was significantly not altered in the rLV-miR-155 + pGFP-V-RS-HGF group, rLV-miR-155 + pGFP-V-RS-c-MET group (Fig. 10I). The Sirt1 promoter luciferase reporter gene activity was significantly increased in the rLV-miR-155 group compared with the rLV group (96625.23 ± 27962.37 vs 780480.19 ± 110346.18, P = 0.002438871 < 0.01). However, it was significantly not altered in the rLV-miR-155 + pGFP-V-RS-HGF group, rLV-miR-155 + pGFP-V-RS-c-MET group (96625.23 ± 27962.37 vs 92502.19 ± 15906.79, P = 0.321743 > 0.05; 96625.23 ± 27962.37vs 89668.56 ± 22722.66, P = 0.07928 > 0.05) (Fig. 10J). The expression of Sirt1 was significantly enhanced in the rLV-miR-155 group compared with the rLV group and reduced in the rLV-Cas9-miR-155 group compared with the rLV-Cas9 group (Fig. 10K **& L**). However, it was significantly not altered in the rLV-miR-155 + pGFP-V-RS-HGF group, rLV-miR-155 + pGFP-V-RS-c-MET group(Fig. 10M**& N**). Collectively, these

results suggest that miR155 promotes Sirt1 expression dependent on HGF-c-MET in human liver cancer stem cells.

miR155 promotes autophagy dependent on Sirt1 in human liver cancer stem cells

Because miR-155 promotes the expression of Sirt1 which can cause the deacetylation of the cellular autophagy structural protein LC3, thereby activating LC3, we will analyze whether miR155 affects the activation of LC3 through Sirt1 in liver cancer stem cells. The binding ability of Sirt1 to LC3 was significantly increased in the rLV-miR-155 group compared with the rLV group and reduced in the rLV-Cas9-miR-155 group compared to the rLV-Cas9 group (Fig. 11A). However, it was significantly not altered in the rLV-miR-155 + NAMPT-NAD + inhibitor group compared to the rLV-Cas9 group (Fig. 11B). The level of acetylation modification of LC3 was significantly reduced in the rLV-miR-155 group compared with the rLV group and increased in the rLV-Cas9-miR-155 group compared to the rLV-Cas9 group (Fig. 11C). However, it was significantly not altered in the rLV-miR-155 + NAMPT-NAD + inhibitor group compared with the rLV group (Fig. 11D**).** The binding ability of LC3 to TP53INP2/DOR was significantly increased in the rLV-miR-155 group compared with the rLV group and reduced in the rLV-Cas9-miR-155 group compared to the rLV-Cas9 group (Fig. 11E). However, it was significantly not altered in the rLV-miR-155 + NAMPT-NAD + inhibitor group and rLV-miR-155 + sirtinol group compared with the rLV group (Fig. 11F). The binding ability of LC3 and ATG4 was significantly increased in the rLV-miR-155 group compared with the rLV group and reduced in the rLV-Cas9-miR-155 group compared to the rLV-Cas9 group (Fig. 11G). However, it was significantly not altered in the rLV-miR-155 + NAMPT-NAD + inhibitor group, rLV-miR-155 + sirtinol group (Fig. 11H**)**. The binding ability of LC3 to ATG3 or ATG7 was significantly increased in the rLV-miR-155 group compared with the rLV group and reduced in the rLV-Cas9-miR-155 group compared to the rLV-Cas9 group (Fig. 11I). However, it was significantly not altered in the rLV-miR-155 + NAMPT-NAD + inhibitor group and rLV-miR-155 + sirtinol group compared with the rLV group (Fig. 11J). The levels of LCI and LC3II (active type) was significantly increased in the rLV-miR-155 group compared with the rLV group and reduced in the rLV-Cas9-miR-155 group compared to the rLV-Cas9 group (Fig. 11K). However, it was significantly not altered in the rLV-miR-155 + NAMPT-NAD + inhibitor group and the rLV-miR-155 + sirtinol group i group compared with the rLV group (Fig. 11L). The interaction between ATG5, ATG12, ATG6L1, and ATG9 was significantly increased in the rLV-miR-155 group compared with the rLV group and reduced in the rLV-Cas9-miR-155 group compared to the rLV-Cas9 group (Fig. 11M). However, it was significantly not altered in the rLV-miR-155 + NAMPT-NAD + inhibitor group and rLV-miR-155 + sirtinol group compared with the rLV group (Fig. 11N). The expression of beclin1 was significantly increased in the rLV-miR-155 group compared with the rLV group and reduced in the rLV-Cas9-miR-155 group compared to the rLV-Cas9 group (Fig. 11O). However, it was significantly not altered in the rLV-miR-155 + NAMPT-NAD + inhibitor group and the rLV-miR-155 + sirtinol group did not change significantly (Fig. 11P). The incidence of autophagy as significantly increased in the rLV-miR-155 group compared with the rLV group(7.63 ± 1.82% vs 35.91 ± 4.36%, P = 0.0042416 < 0.01) and reduced in the rLV-Cas9-miR-155 group compared to the rLV-Cas9 group (8.32 ± 1.067% vs 0.977 ± 0.21%, P = 0.0049583 < 0.01) (Fig. 11**Qa & b**). The incidence

of autophagy as significantly increased in the rLV-miR-155 group compared with the rLV group (9.04 ± 1.67% vs 26.51 ± 3.68%, P = 0.00268 < 0.01). However, it was significantly not altered in the rLV-miR-155 + NAMPT-NAD + inhibitor group and rLV-miR-155 + sirtinol group (9.04 ± 1.67% vs 8.27 ± 1.01%,, P = 0.33331 > 0.05; 9.04 ± 1.67% vs 8.71 ± 1.32%%,, P = 0.431059 > 0.05) (Fig. 11**Ra & b**). The autophagy flow value was significantly decreased in the rLV-miR-155 group compared with the rLV group (183.97 ± 29.21 vs 29.85 ± 4.72, P = 0.007876 < 0.01) and increased in the rLV-Cas9-miR-155 group compared to the rLV-Cas9 group (172.84 ± 17.62 vs 402.82 ± 50.11, P = 0.00851 < 0.01) (Fig. 11S). The autophagy flow value was significantly decreased in the rLV-miR-155 group compared with the rLV group (141.45 ± 21.48 vs 16.46 ± 4.53, P = 0.004659 < 0.01). However, it was significantly not altered in the rLV-miR-155 + NAMPT-NAD + inhibitor group, the rLV-miR-155 + sirtinol group (141.45 ± 21.48 vs 130.71 ± 10.24, P = 0.2136 > 0.05; 139.36 ± 19.15, P = 0.2147 > 0.05) (Fig. 11T). Collectively, these results suggest that miR-155 enhances the occurrence of autophagy through Sirt1 to in liver cancer stem cells.

miR-155 promotes the expression of oncogene H-Ras dependent on autophagy

Given that miR-155 enhances the occurrence of autophagy in liver cancer stem cells, we will analyze whether miR-155 promotes the expression of oncogene H-Ras dependent on autophagy in human liver cancer stem cells.The binding ability of H-Ras to Beclin1, vps34, vps5, Uvrage, bif1, Lamp1, Lamp2, Lamp3, Rubicon, Rab24 was significantly increased in the rLV-miR-155 group compared with the rLV group and reduced in the rLV-Cas9-miR-155 group comoared to the rLV-Cas9 group (Fig. 12A).The expression level of H-Ras was significantly increased in the rLV-miR-155 group compared with the rLV group and reduced in the rLV-Cas9-miR-155 group comoared to the rLV-Cas9 group (Fig. 12B). However, it was significantly not altered in the rLV-miR-155 + 3-MA group compared with the rLV group (Fig. 12C). The expression level of H-Ras was significantly reduced in the rLV-Cas9-miR-155 group compared with the Rlv-Cas9 group. However, it was significantly not altered in the rLV- Cas9-miR-155 + Thapsigargin group compared with the rLV group (Fig. 12D). The binding ability of GTP-Ras or Raf was significantly increased in the rLV-miR-155 group compared with the rLV group and reduced in the rLV-Cas9-miR-155 group comoared to the rLV-Cas9 group (Fig. 12E).However, it was significantly not altered in the rLV-miR-155 + 3-MA group (Fig. 12F).

The expression levels of pRaf1, pMEK1 / 2, pERK1 / 2, pElK, pJak, Jun, pAKT, pmTOR, P70S6K, 4E-BP1, SGK1, and C-myc was significantly increased in the rLV-miR-155 group compared with the rLV group and reduced in the rLV-Cas9-miR-155 group comoared to the rLV-Cas9 group (Fig. 12G). However, it was significantly not altered in the rLV-miR-155 + pGFP-V-RS-H-Ras group compared with the rLV group (Fig. 12H). Collectively, these results suggest that miR155 enhances the expression levels of pRaf1, pMEK1 / 2, pERK1 / 2, pElK, pJak, Jun, pAKT, pmTOR, P70S6K, 4E-BP1, SGK1, C-myc dependent on H-Ras in human human liver cancer stem cells.

H-Ras mediates miR-155 to promote the malignant growth of human liver cancer stem cells

To investigate whether the H-Ras gene plays an important role in the miR-155-induced malignant growth of human liver cancer stem cells, we performed rescued-test. miR-155 ws overexpressed in the rLV-miR-155 group and the rLV-miR-155 + pGFP-V-RS-H-Ras group compared with the rLV group (Fig. 13A-C). The expression of The expression of H-Ras was increased in the rLV-miR-155 group and decreased in rLV-miR-155 + pGFP-V-RS-H-Ras group compared with the rLV group **(**Fig. 13D).The cell growth ability was significantly increased in in the rLV-miR-155 group compared with the rLV group(24th hour: P = 0.00949 < 0.01; 48 hours: P = 0.00936 < 0.01) .However, it was significantly not altered in the rLV-miR-155 + pGFP-V-RS-H-Ras group compared with the rLV group (24 hours: P = 0.2039 > 0.05; 48 hours: P = 0.3564 > 0.05) (Fig. 13E). The BrdU positive rate was significantly increased in in the rLV-miR-155 group compared with the rLV group(17.07 ± 1.47% vs 46.96 ± 6.86%, P = 0.0094 < 0.01).However, it was significantly not altered in the rLV-miR-155 + pGFP-V-RS-H-Ras group compared with the rLV group (17.07 ± 1.47% vs 18.99 ± 5.69%, P = 0.3137 > 0.05) (Fig. 13**Fa & b**). The the colony formation rate was significantly increased in the rLV-miR-155 group compared with the rLV group (31.003 ± 2.88% vs 65.93 ± 10.26%, P = 0.00895 < 0.01).However, it was significantly not altered in the rLV-miR-155 + pGFP-V-RS-H-Ras group compared with the rLV group (31.003 ± 2.88% vs 33.23 ± 5.22%, P = 0.1814 > 0.05) (Fig. 13 **Ga & b)**. The the sphere formation rate was significantly increased in the rLV-miR-155 group compared with the rLV group(13.74 ± 2.74% vs 33.63 ± 5.31%, P = 0.00279 < 0.01).However, it was significantly not altered in the rLV-miR-155 + pGFP-V-RS-H-Ras group compared with the rLV group (13.74 ± 2.74% vs 12.96 ± 2.049%, P = 0.33412 > 0.05) (Fig. 13H). The weight of transplanted tumors was significantly increased in the rLV-miR-155 group compared with the rLV group(0.495 ± 0.088 g vs 0.998 ± 0.205 g, P = 0.00114 < 0.01).However, it was significantly not altered in the rLV-miR-155 + pGFP-V-RS-H-Ras group compared with the rLV group (0.495 ± 0.088 g vs 0.458 ± 0.109 g, P = 0.287409 > 0.05) (Fig. 13I**&J**).The appearance time of transplanted tumors was significantly decreased in the rLV-miR-155 group compared with the rLV group(9.33 ± 1.37 days vs 6 ± 1.095 days, P = 0.28741 < 0.01).However, it was significantly not altered in the rLV-miR-155 + pGFP-V-RS-H-Ras group compared with the rLV group (9.33 ± 1.37 days vs 8.5 ± 1.52, P = 0.2242 > 0.05) (Fig. 13K). The poorly differentiated tumor cells of transplanted tumors was significantly increased in the rLV-miR-155 group compared with the rLV group. However, it was significantly not altered in the rLV-miR-155 + pGFP-V-RS-H-Ras group compared with the rLV group (Fig. 13La). The expression of PCNA in transplanted tumors was significantly increased in the rLV-miR-155 group compared with the rLV group(32.76 ± 6.86% vs 80.67 ± 13.12%, P = 0.00035445 > 0.05).However, it was significantly not altered in the rLV-miR-155 + pGFP-V-RS-H-Ras group compared with the rLV group (32.76 ± 6.86% vs 29.76 ± 8.06%, P = 0.038159 > 0.05) (Fig. 13**La-b &Ma-b**).Collectively, these results suggest that H-Ras knockdown abolished the oncogenic function of miR-155 in liver cancer stem cells.

Discussion

At present, a large number of studies have clarified that miRNA is closely related to tumorigenesis. Our results clearly confirmed that miR-155 is a miRNA closely related to the occurrence and development of liver cancer. In particular, miR-155 promotes the stemness of liver cancer stem cells and the malignant transformation of liver-like cells. Moreover, miR-155 mainly plays a role by triggering autophagy**(Fig. 15**).

A study show that LncRNA MEG3 regulates ALG9 by sponging miR-155(26) and miR-155 regulates the pathogenesis of heart failure(27). These results are consistent with our experimental results. However, miR-155 expression is down-regulated in plasma cells from patients with multiple myeloma, and miR-155 may induce anti-multiple myeloma activity by inhibiting the proteasome(28), indicating that miR-155 is not always play a positive role in carcinogenesis.

Our results have confirmed that miR-155 can target the 3'-UTR of methyltransferase METTL3 and inhibits the expression of METTL3, reducing the binding ability of METTL3 to DNMT1, thereby reducing the m6A methylation modification and stability of the DNMT1 mRNA, resulted in the suppression of DNMT1 transcription and expression, suggesting miR-155 suppressed the expression of DNMT1 dependent on METTL3. More and more studies have shown that METTL3 is involved in the malignant proliferation of tumors by relying on m6A methylation.A heterozygous MBD5 frameshift mutation was found in a family with intellectual disability and epilepsy(29). single-nucleotide variants in MBD5 was associated with autism spectrum disorders and schizophrenia phenotypes(30). Tomato MBD5 interacts with UV-damaged DNA binding protein-1(31). m6A RNA methylation regulators correlate with malignant progression(32) **and** METTL3 inhibits PI3K/Akt signaling pathway(33). At present, there are few reports about miR-155 regulating the m6A methylation modification of DNMT1 mRNA through METTL3, and its specific mechanism still needs to be further clarified.

Our research found that miR-155 can alter the DNA methylation modification in human liver cancer stem cells. The main mechanisms are as follows: (a) miR-155 targets methyl-CpG binding domain protein 5 (MBD5) and inhibits MBD5 Expression. (b) miR-155 targets METTL3 and inhibits METTL3 expression, and further reduces DNMT1 expression. (c) miR-155 inhibits the interaction between MBD5 and DNMT1 in liver cancer stem cells, thereby reducing The binding ability between MBD5, DNMT1 and the three DNA methylation binding regions of IGFII (H19 ICR, IGFII DMR, IGFII Enhancer). (4) The results of specific methylation PCR and DpnI methylation PCR showed miR-155 inhibition the methylation modification levels of the three DNA methylation binding regions of IGFII (H19 ICR, IGFII DMR, IGFII Enhancer) are shown. Studies have shown that MBD5 may contribute to the formation or function of heterochromatin (34). In particular, our results also confirm that miR-155 can reduce the interaction between MBD5 and DNMT1. miR-155 reduced the expression of DNA methyltransferase DNMT1 and the interaction between MBD5 and DNMT1 in human liver cancer stem cells by inhibiting METTL3.LINP1 promotes the progression of cervical cancer by scaffolding EZH2, LSD1 and DNMT1 (35). These results suggest that miR-155 inhibits the binding ability of MBD5 or DNMT1 to the three DNA methylation binding sequences (H19 ICR, IGFII DMR, IGFII Enhancer) in liver cancer stem cells.

Our results suggest that miR155 enhances IGFII expression through the IGFII DNA loop in human liver cancer stem cells. Insulin-like growth factor II (IGFII) acts as a potent mitogen for several tumor types. Matrix metalloproteinase-9 interplays with the IGFBP2-IGFII complex to promote cell growth and motility (36). EphB4 phosphodegron was regulated by the autocrine IGFII in malignant mesothelioma(37). Long noncoding RNA HULC accelerates the growth of human liver cancer stem cells by miR675-PKM2 pathway(38). Histone 3 lysine 9 dimethylation (H3K9me2) orchestrates inheritance of spatial positioning

of peripheral heterochromatin through mitosis (39). Abo1 is required for the H3K9me2 to H3K9me3 transition in heterochromatin(40).

Notably, our findings show that miR155 promotes the expression of hepatocyte growth factor HGF dependent on IGFII in human liver cancer stem cells. These results suggest that miR155 promotes Sirt1 expression dependent on HGF-c-MET. HGF regulates myoblast migration(41).Selective MET inhibitors inhitits non-small cell lung cancer with MET exon 14 skipping (42). HGF-PARP-1 signaling promotes invasion of ovarian cancer cells(43). Anti-tumor activity of Bufalin by inhibiting c-MET mediated MEK/ERK Pathways (44). The C-reactive protein/albumin (CRP/Alb) ratio is a novel inflammation-based score in pancreatic cancer(45). Alb is association with IL-12 levels(46).

Our results have clearly shown that miR-155 affects the production and function of autophagy in liver cancer stem cells. Our results indicate that miR-155 activates LC3 and promotes the formation of autophagy. First of all, our study found that miR-155 promoted the binding of IGFII to stemness factors and loaded the stemness factors into the HGF promoter region of hepatocyte growth factor, which enhanced the transcriptional activity of HGF and promoted the expression of HGF. miR-155 significantly enhances the transcription and expression ability of HGF denpendent on IGFII. Further research shows that miR-155 promotes HGF-MET-mediated albumin gene (ALB) transcription and translation, and significantly promotes Sirt1 transcription and expression through ALB. After Sirt1 expression increases, miR-155 relies on Sirt1 to promote The deacetylation of LC3 in the nucleus enhanced the binding of LC3 to TP53INP2/DOR, resulting in LC3 nucleation. Our results also show that miR-155 promotes the binding of LC3 and ATG4 in the cytoplasm, which causes LC3 to form LC3-I under the processing of ATG4. Immediately thereafter, the binding ability of LC3 to ATG3 and ATG7 is significantly enhanced, and the results of western blotting show The level of LC3-II increased significantly, indicating that overexpression of miR-155 activated LC3 through the above mechanism. It is meaningful that the level of LC3-II did not increase significantly after the addition of Sirt1 inhibitor, suggesting that miR-155 to promote Activation of LC3 dependent on Sirt1. Studies have reported that miR-155 induces the occurrence of autophagy by regulating the expression of autophagy-related genes(47), which is consistent with our research results, suggesting that miR-155 activates LC3 by affecting the expression of Sirt1, thereby inducing the occurrence of autophagy.

Since overexpression of miR-155 activates LC3 in liver cancer stem cells, miR-155 is likely to also promote the assembly of autophagosomes. In fact, our results have shown that excessive miR-155 enhances the interaction between ATG5 and ATG12, ATG16L1 and ATG9. and miR-155 can promote the occurrence of autophagy. Studies have shown that the assembly of autophagosomes mainly includes three steps: the initiation, nucleation and amplification of the separation membrane, and involves the participation of three complexes, namely the ULK1 complex (ULK1, FIP200, ATG13 and ATG101), PI3KC3 complex (Beclin-1, VPS34, VPS15 and ATG14L) and ATG16L1 complex (ATG16L1, ATG5 and ATG12)(48). Although our research shows that miR-155 can promote the assembly of autophagosomes, the exact mechanism of how miR-155 regulates the assembly of autophagosomes is not clear, and further research is needed.

Several studies suggest that senescent stromal cells promote cancer resistance dependent on SIRT1 loss(49). Inhibiting SIRT1 by SMURF2 suppresses CRC cell proliferation(50).Our results suggest that miR-155 enhances the occurrence of autophagy through Sirt1 in liver cancer stem cells.Autophagy proved beneficial in evading various foreign pathogens in the context of cancer(51). TP53INP2/DOR protein chaperones deacetylated nuclear LC3 to the cytoplasm to promote macroautophagy(52). LC3-Dependent EV Loading and Secretion (LDELS) is distinct from classical macroautophagy/autophagy(53). Hypoxia-induced acetylation of PAK1 enhances autophagy and promotes brain tumorigenesis via phosphorylating ATG5(54). autophagy pathway and are involved in autophagy initiation, nucleation, elongation, maturation, fusion and degradation(55). ATG9A supplies PtdIns4P to the autophagosome initiation site(56). SETD2 mutation in renal clear cell carcinoma suppress autophagy via regulation of ATG12(57).

Cellular autophagy can be selectively degraded by autophagy receptors, and then play a role in selectively removing damaged organelles and specific proteins. p62 (SQSTM1) is a receptor involved in selective autophagy (58), suggesting that autophagy Phagocytosis can play a role in selective degradation.We found that miR-155 may achieve the selectivity for oncoprotein H-Ras by regulating the occurrence of cellular autophagy. Our results show that miR-155 enhances the binding ability of H-Ras and Beclin1, Vps34, Vps15, Uvrage, Bif1, Lamp1, Lamp2, Lamp3, Rubicon, Rab24 in autophagosomes. miR-155 promoted the expression of H-Ras, suggesting that miR-155 enhances the H-Ras expression dependent on cell autophagy. MicroRNA-30a targets BECLIN-1 to inactivate autophagy and sensitizes gastrointestinal stromal tumor cells to imatinib(59) .Accumulating evidence indicates that Vps34 may also contribute to the progression of human cancers and stimulates the p62 phosphorylation(60). UVRAG is one of the key players of autophagy(61). RAB24 has also been connected to several diseases including ataxia, cancer and tuberculosis(62). Our results are likely to lay some foundation for revealing the new function of autophagy, which still needs further study.

Our results show that in human liver cancer stem cells, miR-155 stabilizes the MAPK signaling pathway by activating H-Ras. The main molecular mechanisms involved are as follows: (1) miR-155-dependent cell autophagy enhances H in human liver cancer stem cells -Ras expression; (2) miR-155 enhanced the binding ability of GTP-Ras and Raf1, and after adding autophagy inhibitors, the binding ability of GTP-Ras and Raf1 did not increase significantly, suggesting that miR-155 dependent cell self Phagocytosis enhanced the binding ability of GTP-Ras to Raf1, indicating that miR-155 activated H-Ras; (3) overexpression of miR-155 also significantly increased pRaf1, pMEK1/2, pERK1/2, pElK, pJak, Jun, pAKT, pmTOR, P70S6K, 4E-BP1, SGK1, C-myc levels, and after transfer into the H-Ras interference plasmid, pRaf1, pMEK1/2, pERK1/2, pElK, pJak, Jun, pAKT, pmTOR, P70S6K, 4E-BP1, SGK1, C-myc levels did not change significantly, suggesting that miR-155 relies on H-Ras to enhance pRaf1, pMEK1/2, pERK1/2, pElK, pJak, Jun, pAKT, pmTOR, The levels of P70S6K, 4E-BP1, SGK1, and C-myc indicate that miR-155 enhances the function of H-Ras and relies on H-Ras to activate the MAPK signaling pathway. Oncogene H-Ras is an important component of many signaling pathways in cells and plays a key role in tumorigenesis and development. Research reports that H-Ras can interact with Raf and induce Raf and ERK phosphorylation, thereby activating MAPK signaling pathway, our results are consistent with literature reports. Studies have shown that abnormal activation of H-Ras and MAPK signaling pathways

often occurs in tumors, and MAPK signaling pathways are activated in most liver cancers. Our results also show that miR-155 activates the MAPK signaling pathway through H-Ras and thus promotes the malignant growth of human liver cancer stem cells.H-Ras is a unique isoform of the Ras GTPase family, one of the most prominently mutated oncogene families across the cancer landscape(63). H-Ras activation promotes invasion in cutaneous squamous cell carcinoma(64).RAF1 rearrangements are common in pancreatic acinar cell carcinomas(65). MEK1/2 inhibitors suppresses cancer growth in mice(66) **and** circ-0000745 enhanced cerll proliferation by activating ERK pathway(67). C-jun is activated in renal cell carcinoma(68). MicroRNA-493-5p suppresses colorectal cancer progression via the PI3K-Akt-FoxO3a signaling pathway(69). ANXA6 contributes to radioresistance by promoting autophagy via inhibiting the PI3K/AKT/**mTOR** signaling pathway in nasopharyngeal carcinoma(70). Recently, 4E-BP1 was shown to be phosphorylated by other kinases besides mTOR, and overexpression of 4E-BP1 was found in different human carcinomas(71). SGK1 inhibition induces autophagy-dependent apoptosis via the mTOR-Foxo3a pathway(72).c-myc contributes to neoplastic transformation and induces genomic instability(73). These results suggest that H-Ras knockdown abolished the oncogenic function of miR-155 in liver cancer stem cells.

In this study, we reveal some of the cellular molecular mechanisms by which miR-155 plays a carcinogenic role in the development of human liver cancer, but the exact molecular mechanisms of many processes need to be further confirmed, including: (a) Further verification of miR-155 tumorigenicity. (b) Further Clarify how miR-155 enhances the stemness of cells and how miR-155 regulates dryness factors, such as Oct4, Nanog, C-myc, Sox2, etc. (c) The mechanism of miR-155 regulating cell autophagy needs further study, especially how miR-155 can accurately regulate the assembly of intracellular autophagosomes and the selective treatment ability of proteins such as proteins by autophagy. In conclusions, it further provides a basis for the screening of clinical liver cancer diagnostic markers and the selection of drug treatment targets.

Conclusions

We reveal some of the cellular molecular mechanisms by which miR-155 plays a carcinogenic role in the development of human liver cancer, but the exact molecular mechanisms of many processes need to be further confirmed, including: (a) Further verification of miR-155 tumorigenicity. (b) Further Clarify how miR-155 enhances the stemness of cells and how miR-155 regulates dryness factors, such as Oct4, Nanog, C-myc, Sox2, etc. (c) The mechanism of miR-155 regulating cell autophagy needs further study, especially how miR-155 can accurately regulate the assembly of intracellular autophagosomes and the selective treatment ability of proteins such as proteins by autophagy. In conclusions, it further provides a basis for the screening of clinical liver cancer diagnostic markers and the selection of drug treatment targets.

Abbreviations

chaperone-mediated autophagy (CMA)

Methyltransferase 3 (METTL3)

Sodium dodecyl sulfate-polyacrylamide gel electrophoresis (SDS-PAGE)

RNA Immunoprecipitation(RIP)

Chromosome conformation capture (3C)

Methyl-CpG-binding domain protein 5 (MBD5)

RNA Methyltransferase-Like Protein3 (METTL3)

methyl-CpG binding domain protein 5 (MBD5)

Insulin-like growth factor II (IGFII)

Histone 3 lysine 9 dimethylation (H3K9me2)

Declarations

Ethics approval and consent to participate

All methods were carried out in "accordance" with the approved guidelines. All experimental protocols "were approved by" a Tongji university institutional committee. Informed consent was obtained from all subjects. The study was reviewed and approved by the China national institutional animal care and use committee.

Consent for publication

'Not applicable'

Availability of data and material

'Not applicable'

Competing interests

"The authors declare that they have no competing interests"

Funding: This study was supported by grants from National Natural Science Fundation of China (NCSF No.8127229181773158) and by grants from Science and Technology Commission of Shanghai Municipality Basic Research Field Project□19JC1415200□.

Authors' contributions: Dongdong Lu conceived the study and participated in the study design, performance, coordination and manuscript writing. Xiaoxue Jiang, Yanan Lu, Shuting Song, Yingjie Chen, Sijie Xie, Liyan Wang, performed the research. All authors have read and approved the final manuscripts.

Acknowledgements: This study was supported by grants from National Natural Science Fundation of China (NCSF No.8127229181773158) and by grants from Science and Technology Commission of Shanghai Municipality Basic Research Field Project（19JC1415200）.

References

1. Volinia S, Calin GA, Liu CG, et al. A microRNA expression signature of human solid tumors defines cancer gene targets. Proc Natl Acad Sci U S A. 2006;103(7):2257–61.
2. Liu D, Han P, Gao C, Gao W, Yao X, Liu S. microRNA-155 Modulates Hepatic Stellate Cell Proliferation, Apoptosis, and Cell Cycle Progression in Rats With Alcoholic Hepatitis *via* the MAPK Signaling Pathway Through Targeting SOCS1 Front Pharmacol. 2020;11:270.
3. Kirave P, Gondaliya P, Kulkarni B, Rawal R, Garg R, Jain A, Kalia K. Exosome mediated miR-155 delivery confers cisplatin chemoresistance in oral cancer cells via epithelial-mesenchymal transition.Oncotarget. 2020;11(13):1157–1171.
4. Ruan Z, Chu T, Wu L, Zhang M, Zheng M, Zhang Q, Zhou M, Zhu G. miR-155 inhibits oxidized low-density lipoprotein-induced apoptosis in different cell models by targeting the p85α/AKT pathway.J Physiol Biochem. 2020 Apr 10. doi: 10.1007/s13105-020-00738-0.
5. Huang J, Weng Q, Shi Y, Mao W, Zhao Z, Wu R, Ren J, Fang S, Lu C, Du Y, Ji J. MicroRNA-155-5p suppresses PD-L1 expression in lung adenocarcinoma.FEBS Open Bio. 2020. doi: 10.1002/2211-5463.
6. Chen G, Chen Z, Zhao H. MicroRNA-155-3p promotes glioma progression and temozolomide resistance by targeting Six1J Cell Mol Med. 2020. doi: 10.1111/jcmm.15192.
7. Hong Y, He H, Jiang G, Zhang H, Tao W, Ding Y, Yuan D, Liu J, Fan H, Lin F, Liang X, Li X, Zhang Y. miR-155-5p inhibition rejuvenates aged mesenchymal stem cells and enhances cardioprotection following infarction. Aging Cell. 2020;19(4):e13128.
8. Cuervo AM, Wong E. Chaperone-mediated autophagy: roles in disease and aging. Cell Res. 2014;24(1):92–104.
9. Lamb CA, Yoshimori T, Tooze SA. The autophagosome: origins unknown, biogenesis complex. Nat Rev Mol Cell Biol. 2013;14(12):759–74.
10. Walczak M, Martens S. Dissecting the role of the Atg12-Atg5-Atg16 complex during autophagosome formation. Autophagy. 2013;9(3):424–5.
11. Pankiv S, Clausen TH, Lamark T, et al. p62/SQSTM1 binds directly to Atg8/LC3 to facilitate degradation of ubiquitinated protein aggregates by autophagy. J Biol Chem. 2007;282(33):24131–45.
12. Thurston TL, Wandel MP, von Muhlinen N, et al. Galectin 8 targets damaged vesicles for autophagy to defend cells against bacterial invasion. Nature. 2012;482(7385):414–8.
13. Hendrich B, Bird A. Identification and characterization of a family of mammalian methyl-CpG binding proteins. Mol Cell Biol. 1998;18(11):6538–47.

14. Mullegama SV, Pugliesi L, Burns B, et al. MBD5 haploinsufficiency is associated with sleep disturbance and disrupts circadian pathways common to Smith-Magenis and fragile X syndromes. Eur J Hum Genet. 2015;23(6):781–9.
15. Haussmann IU, Bodi Z, Sanchez-Moran E, et al. m(6)A potentiates Sxl alternative pre-mRNA splicing for robust Drosophila sex determination. Nature. 2016;540(7632):301–4.
16. Ke S, Alemu EA, Mertens C, et al. A majority of m6A residues are in the last exons, allowing the potential for 3' UTR regulation. Genes Dev. 2015;29(19):2037–53.
17. Kennedy EM, Bogerd HP, Kornepati AV, et al. Posttranscriptional m(6)A Editing of HIV-1 mRNAs Enhances Viral Gene Expression. Cell Host Microbe. 2016;19(5):675–85.
18. Wang X, Zhao BS, Roundtree IA, et al. N(6)-methyladenosine Modulates Messenger RNA Translation Efficiency. Cell. 2015;161(6):1388–99.
19. Alarcon CR, Lee H, Goodarzi H, et al. N6-methyladenosine marks primary microRNAs for processing. Nature. 2015;519(7544):482–5.
20. Bostick M, Kim JK, Esteve PO, et al. UHRF1 plays a role in maintaining DNA methylation in mammalian cells. Science. 2007;317(5845):1760–4. S.
21. Pathania R, Ramachandran S, Elangovan S, et al. DNMT1 is essential for mammary and cancer stem cell maintenance and tumorigenesis. Nat Commun. 2015;6:6910–36.
22. Werner H, LeRoith D. Insulin and insulin-like growth factor receptors in the brain: physiological and pathological aspects. Eur Neuropsychopharmacol. 2014;24(12):1947–53.
23. Trusolino L, Bertotti A, Comoglio PM. MET signalling: principles and functions in development, organ regeneration and cancer. Nat Rev Mol Cell Biol. 2010;11(12):834–48.
24. Lam BQ, Dai L, Qin Z. The role of HGF/c-MET signaling pathway in lymphoma. J Hematol Oncol. 2016;9(1):135–42.
25. Simanshu DK, Nissley DV, McCormick F. RAS Proteins Their Regulators in Human Disease Cell. 2017;170(1):17–33.
26. Yu Y, Kou D, Liu B, Huang Y, Li S, Qi Y, Guo Y, Huang T, Qi X, Jia L. LncRNA MEG3 contributes to drug resistance in acute myeloid leukemia by positively regulating ALG9 through sponging miR-155. Int J Lab Hematol. 2020. doi:10.1111/ijlh.13225.
27. Li J, Su H, Zhu Y, Cao Y, Ma X. ETS2 and microRNA-155 regulate the pathogenesis of heart failure through targeting and regulating GPR18 expression. Exp Ther Med. 2020;19(6):3469–78.
28. Amodio N, Gallo Cantafio ME, Botta C, et al. Replacement of miR-155 Elicits Tumor Suppressive Activity and Antagonizes Bortezomib Resistance in Multiple Myeloma. Cancers (Basel). 2019;11(2):236–51.
29. Han JY, Lee IG, Jang W, Kim M, Kim Y, Jang JH, Park J. Diagnostic exome sequencing identifies a heterozygous MBD5 frameshift mutation in a family with intellectual disability and epilepsy. Eur J Med Genet. 2017 Oct;60(10):559–64.

30. Ishizuka K, Kimura H, Yoshimi A, Banno M, Kushima I, Uno Y, Okada T, Mori D, Aleksic B, Ozaki N. Investigation of single-nucleotide variants in MBD5 associated with autism spectrum disorders and schizophrenia phenotypes. Nagoya J Med Sci. 2016;78(4):465–74.
31. Li Y, Deng H, Miao M, Li H, Huang S, Wang S, Liu Y. Tomato MBD5, a methyl CpG binding domain protein, physically interacting with UV-damaged DNA binding protein-1, functions in multiple processes New Phytol. 2016 Apr;210(1):208–26.
32. Zhang QJ, Luan JC, Song LB, Cong R, Ji CJ, Zhou X, Xia JD, Song NH. m6A RNA methylation regulators correlate with malignant progression and have potential predictive values in clear cell renal cell carcinoma Exp Cell Res. 2020 Apr 22:112015. doi: 10.1016/j.yexcr.2020.112015.
33. Ji JW, Zhang YD, Lai YJ, Huang CG. Mettl3 regulates the proliferation, migration and invasion of glioma cells by inhibiting PI3K/Akt signaling pathway. Eur Rev Med Pharmacol Sci. 2020;24(7):3818–28.
34. Laget S, Joulie M, Le Masson F, et al. The human proteins MBD5 and MBD6 associate with heterochromatin but they do not bind methylated DNA. PLoS One. 2010;5(8):e11982.
35. Wu L, Gong Y, Yan T, Zhang H. LINP1 Promotes the Progression of Cervical Cancer by Scaffolding EZH2, LSD1 and DNMT1 to Inhibit the Expression of KLF2 and PRSS8.Biochem Cell Biol. 2020 Apr 29. doi: 10.1139/bcb-2019-0446.
36. Rorive S, Berton A, D'haene N, Takacs CN, Debeir O, Decaestecker C. Salmon I.Matrix metalloproteinase-9 interplays with the IGFBP2-IGFII complex to promote cell growth and motility in astrocytomas. Glia. 2008;56(15):1679–90.
37. Scalia P, Pandini G, Carnevale V, Giordano A, Williams SJ. Identification of a novel EphB4 phosphodegron regulated by the autocrine IGFII/IR_A axis in malignant mesothelioma.Oncogene. 2019;38(31):5987–6001.
38. Wang C, Jiang X, Li X, Song S, Meng Q, Wang L, Lu Y, Xin X, Pu H, Gui X, Li T, Lu D. Long noncoding RNA HULC accelerates the growth of human liver cancer stem cells by upregulating CyclinD1 through miR675-PKM2 pathway via autophagy. Stem Cell Res Ther. 2020 Jan;3(1):8. 11(.
39. Poleshko A, Smith CL, Nguyen SC, Sivaramakrishnan P, Wong KG, Murray JI, Lakadamyali M, Joyce EF, Jain R. Epstein JA.H3K9me2 orchestrates inheritance of spatial positioning of peripheral heterochromatin through mitosis. Elife. 2019;8:pii: e49278.
40. Dong W, Oya E, Zahedi Y, Prasad P, Svensson JP, Lennartsson A, Ekwall K, Durand-Dubief M. Abo1 is required for the H3K9me2 to H3K9me3 transition in heterochromatin. Sci Rep. 2020;10(1):6055.
41. Roveimiab Z, Lin F, Anderson JE. Traction and attraction: Haptotaxis substrates collagen and fibronectin interact with chemotaxis by HGF to regulate myoblast migration in a microfluidic device. Am J Physiol Cell Physiol. 2020. doi:10.1152/ajpcell.00417.2019.
42. Salgia R, Sattler M, Scheele J, Stroh C, Felip E. The promise of selective MET inhibitors in non-small cell lung cancer with MET exon 14 skipping.Cancer Treat Rev. 2020 Apr 9;87:102022.
43. Wei W, Lv S, Zhang C, Tian Y. Potential role of HGF-PARP-1 signaling in invasion of ovarian cancer cells. Int J Clin Exp Pathol. 2018;11(7):3310–7.

44. Qian L, Su H, Wang G, Li B, Shen G, Gao Q. Anti-tumor Activity of Bufalin by Inhibiting c-MET Mediated MEK/ERK and PI3K/AKT Signaling Pathways in Gallbladder. Cancer J Cancer. 2020;11(11):3114–23.
45. Liu Z, Jin K, Guo M, Long J, Liu L, Liu C, Xu J, Ni Q, Luo G, Yu X. Prognostic Value of the CRP/Alb Ratio, a Novel Inflammation-Based Score in Pancreatic Cancer. Ann Surg Oncol. 2017;24(2):561–8.
46. Ma Z, Lu D, Zhao W, Wang HRBP. and Alb in neonatal hydronephrosis and its association with IL-12 levels in pregnant women before delivery. Exp Ther Med. 2019;18(1):497–502.
47. Wan G, Xie W, Liu Z, et al. Hypoxia-induced MIR155 is a potent autophagy inducer by targeting multiple players in the MTOR pathway. Autophagy. 2014;10(1):70–9.
48. Lamb CA, Yoshimori T, Tooze SA. The autophagosome: origins unknown, biogenesis complex. Nat Rev Mol Cell Biol. 2013;14(12):759–74.
49. Han L, Long Q, Li S, Xu Q, Zhang B, Dou X, Qian M, Jiramongkol Y, Guo J, Cao L, Chin YE, Lam EW, Jiang J, Sun Y. Senescent stromal cells promote cancer resistance through SIRT1 loss-potentiated overproduction of small extracellular vesicles.Cancer Res. 2020. pii: canres.0506.2020.
50. 10.1038/s41388-020-1298-0
Yu L, Dong L, Li H, Liu Z, Luo Z, Duan G, Dai X, Lin Z. Ubiquitination-mediated degradation of SIRT1 by SMURF2 suppresses CRC cell proliferation and tumorigenesis.Oncogene. 2020 May 2. doi:10.1038/s41388-020-1298-0.
51. Panigrahi 51SahaS, Patil DP, Bhutia S. SK. Autophagy in health and disease: A comprehensive review.Biomed Pharmacother. 2018;104:485–495.
52. Liu X, Klionsky DJ. TP53INP2/DOR protein chaperones deacetylated nuclear LC3 to the cytoplasm to promote macroautophagy.Autophagy. 2015;11(9):1441–2.
53. Leidal AM, Debnath J. LC3-dependent extracellular vesicle loading and secretion (LDELS).Autophagy. Apr. 2020;24:1–2. doi:10.1080/15548627.2020.1756557.
54. Feng X, Zhang H, Meng L, Song H, Zhou Q, Qu C, Zhao P, Li Q, Zou C, Liu X, Zhang Z. Hypoxia-induced acetylation of PAK1 enhances autophagy and promotes brain tumorigenesis via phosphorylating ATG5. Autophagy. 2020 Mar 18:1–20. doi: 10.1080/15548627.2020.
55. Li X, He S, Ma B. Autophagy and autophagy-related proteins in cancer. Mol Cancer. 2020;19(1):12.
56. Judith D, Tooze SA. ATG9A supplies PtdIns4P to the autophagosome initiation site.Autophagy. 2019;15(9):1660–1661.
57. González-Rodríguez P, Engskog-Vlachos P, Zhang H, Murgoci AN, Zerdes I, Joseph B. SETD2 mutation in renal clear cell carcinoma suppress autophagy via regulation of ATG12.Cell Death Dis. 2020;11(1):69.
58. Liu KK, Qiu WR, Naveen Raj E, et al. Ubiquitin-coated nanodiamonds bind to autophagy receptors for entry into the selective autophagy pathway. Autophagy. 2017;13(1):187–200.
59. Chen W, Li Z, Liu H, Jiang S, Wang G, Sun L, Li J, Wang X, Yu S, Huang J, Dong Y. MicroRNA-30a targets BECLIN-1 to inactivate autophagy and sensitizes gastrointestinal stromal tumor cells to

imatinib. Cell Death Dis. 2020;11(3):198.

60. Jiang X, Bao Y, Liu H, Kou X, Zhang Z. VPS34 stimulation of p62 phosphorylation for cancer progression. Oncogene. 2017;36(50):6850–62.
61. Song Y, Quach C, Liang C. UVRAG in autophagy, inflammation, and cancer.Autophagy. 2020;16(2):387–388.
62. Ylä-Anttila P, Eskelinen EL. Roles for RAB24 in autophagy and disease ã□□Small GTPases. 2018;9(1–2):57–65.
63. Shu L, Wang D, Saba NF, Chen ZG. A Historic Perspective and Overview of H-Ras Structure, Oncogenicity, and Targeting. Mol Cancer Ther. 2020;19(4):999–1007.
64. Siljamäki E, Rappu P, Riihilä P, Nissinen L, Kähäri VM, Heino J. H-Ras activation and fibroblast-induced TGF-β signaling promote laminin-332 accumulation and invasion in cutaneous squamous cell carcinoma.Matrix Biol. 2020 May;87:26–47.
65. 10.1038/s41379-020-0545-9
Prall OWJ, Nastevski V, Xu H, McEvoy CRE, Vissers JHA, Byrne DJ, Takano E, Yerneni S, Ellis S, Green T, Mitchell CA, Murray WK, Scott CL, Grimmond SM, Hofmann O, Papenfuss A, Kee D, Fellowes A, Brown IS, Miller G, Kumarasinghe MP, Perren A, Nahm CB, Mittal A, Samra J, Ahadi M, Fox SB, Chou A, Gill AJ. RAF1 rearrangements are common in pancreatic acinar cell carcinomas.Mod Pathol. 2020 May 1. doi: 10.1038/s41379-020-0545-9.
66. Brown CN, Atwood DJ, Pokhrel D, Ravichandran K, Holditch SJ, Saxena S, Miyazaki M, Nemenoff R, Weiser-Evans MCM, Ljubanovic DG, Joy MS, Edelstein CL. The effect of MEK1/2 inhibitors on cisplatin-induced acute kidney injury (AKI) and cancer growth in mice. Cell Signal. 2020;71:109605.
67. Liu X, Zhou C, Li Y, Deng Y, Lu W, Li J. Upregulation of circ-0000745 in acute lymphoblastic leukemia enhanced cerll proliferation by activating ERK pathway.Gene. 2020 Apr 30:144726. doi: 10.1016/j.gene.2020.144726.
68. Oya M, Mikami S, Mizuno R, Marumo K, Mukai M, Murai M. C-jun activation in acquired cystic kidney disease and renal cell carcinoma.J Urol. 2005 Aug;174(2):726.
69. Cui FC, Chen Y, Wu XY, Hu M, Qin WS. MicroRNA-493-5p suppresses colorectal cancer progression via the PI3K-Akt-FoxO3a signaling pathway. Eur Rev Med Pharmacol Sci. 2020;24(8):4212–23.
70. Chen Q, Zheng W, Zhu L, Yao D, Wang C, Song Y, Hu S, Liu H, Bai Y, Pan Y, Zhang J, Guan J, Shao C. ANXA6 Contributes to Radioresistance by Promoting Autophagy via Inhibiting the PI3K/AKT/mTOR Signaling Pathway in Nasopharyngeal Carcinoma. Front Cell Dev Biol. 2020;8:232.
71. Qin X, Jiang B, Zhang Y. E-BP1, a multifactor regulated multifunctional protein. Cell Cycle. 2016;4(6):781–6. 15(.
72. Liu W, Wang X, Liu Z, Wang Y, Yin B, Yu P, Duan X, Liao Z, Chen Y, Liu C, Li X, Dai Y, Tao Z. SGK1 inhibition induces autophagy-dependent apoptosis via the mTOR-Foxo3a pathway. Br J Cancer. 2017;117(8):1139–53.
73. Mai S, Mushinski JF. c-Myc-induced genomic instability. J Environ Pathol Toxicol Oncol. 2003;22(3):179–99.

74. Liu X, Zhou Y, Peng J, Xie B, Shou Q, Wang J. Silencing c-Myc Enhances the Antitumor Activity of Bufalin by Suppressing the HIF-1α/SDF-1/CXCR4 Pathway in Pancreatic Cancer Cells.Front Pharmacol. 2020 Apr 17;11:495.
75. Chen H, Guo Y, Sun J, Dong J, Bao Q, Zhang X, Fu F. Preferential Expression of B7-H6 in Glioma Stem-Like Cells Enhances Tumor Cell Proliferation via the c-Myc/RNMT Axis. J Immunol Res. 2020;2020:2328675.

Figures

Figure 1

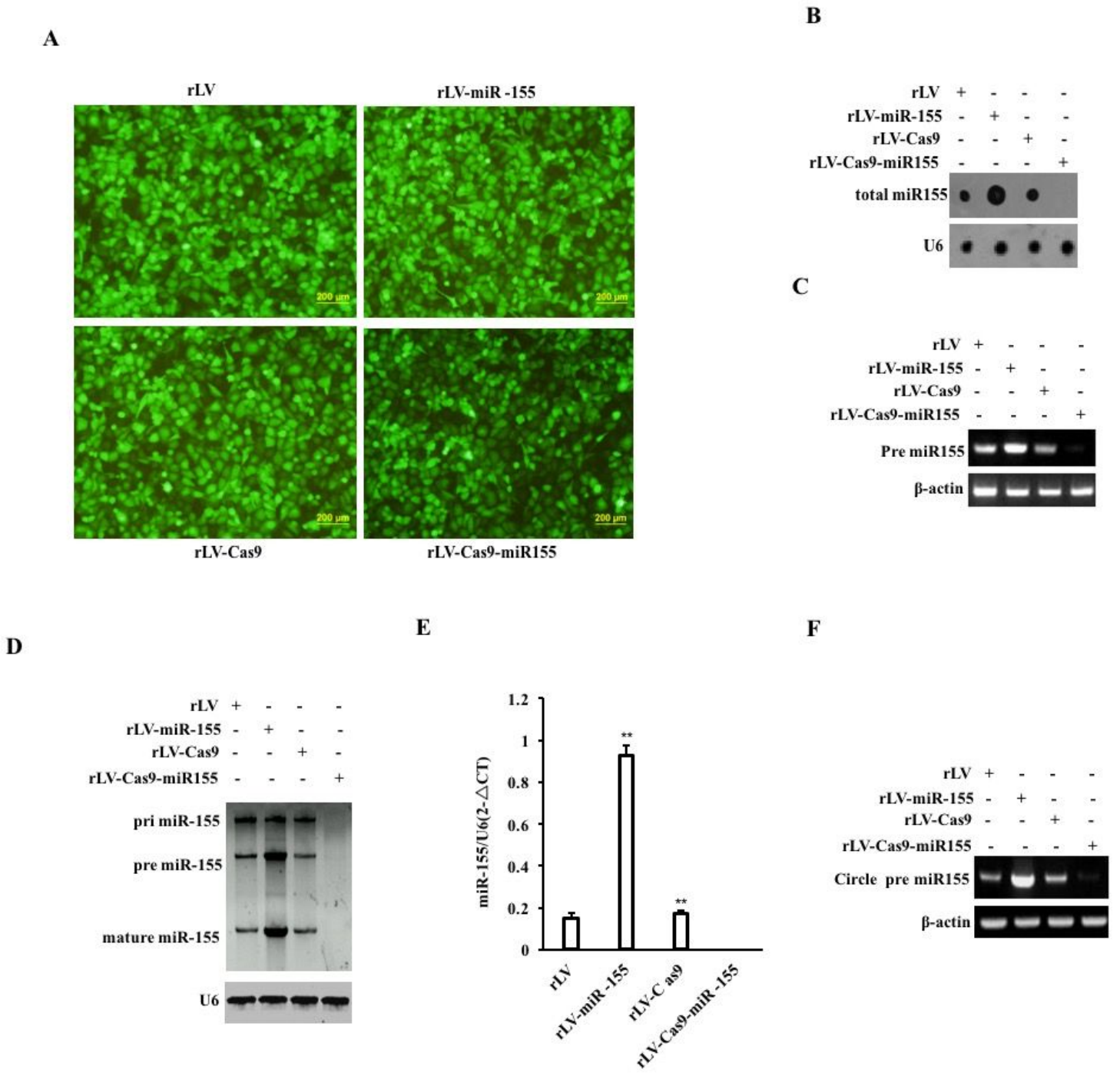

Figure 1

Construction and identification of miR-155 overexpressed and knocked- out human liver cancer stem cell lines. A. Image taken with a fluorescence microscope (100x). B. Dot-Blot was used to detect miR-155 in the cells, and U6 was used as the internal reference gene. C. Detect miR-155 precursors in cells using transcription polymerase chain reaction (RT-PCR) with β-actin as an internal reference gene. D. Northern blotting (Northern blotting) was used to detect the precursors, precursors and matures of miR-155 in the cells, and U6 was used as the internal reference gene. E. The quantitative reverse transcription

polymerase chain reaction (RT-PCR) was used. The mature body of miR-155 was detected in the cells, and U6 was used as an internal reference gene. F. Detection of circular miR-155 in cells using back-to-back RT-PCR.

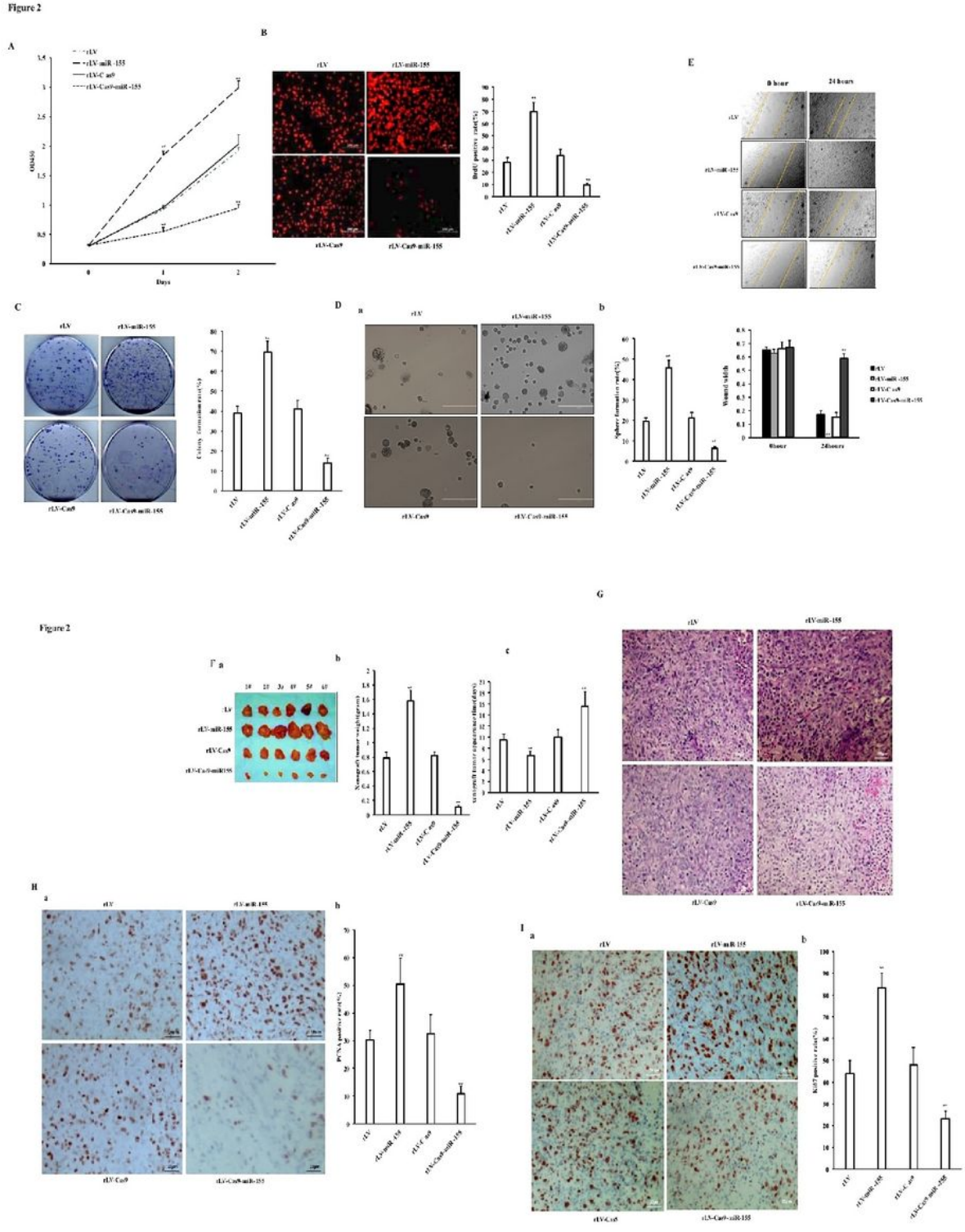

Figure 2

Effect of miR-155 on the growth of liver cancer stem cells in vitro and in vivo. A. The growth curve of hLCSCs cells in vitro (CCK8 method). B. Determination of S-phase of hLCSCs cells by BrdU staining. a.

BrdU staining photos; b. Determine the percentage of cell S phase of these stably transfected cell lines. C. Cell plate colony forming ability assay. a. Photo of plate colonies; b. cell plate colony formation rate. D. Sphere formation ability of hLCSCs cells. a. Sphere photographs of hLCSCs cells. b. Sphere formation rate (%). E. Cell scratching ability determination. a. Photos taken at 0 and 24 hours, respectively. b. Comparison of the average scratch width of hLCSCs cells. F. a. Photographs of xenograft. b. Comparison of size (g) of transplanted tumors in nude mice. c. Comparison of the transplanted tumor appearance time(days). G. 4% formaldehyde-fixed paraffin-embedded nude mice transplanted tumor tissue sections (4 μm) were subjected to hematoxylin-eosin (HE) (original magnification × 100). H. a. Anti-PCNA immunohistochemical staining (original magnification × 100). b Comparison of PCNA positive rate. c. Western blotting was used to detect the expression of PCNA, β-actin was used as the internal reference gene. I. a. Immunohistochemical staining of anti-Ki67 (original magnification × 100). B. Comparison of Ki67 positive rate.

Figure 3

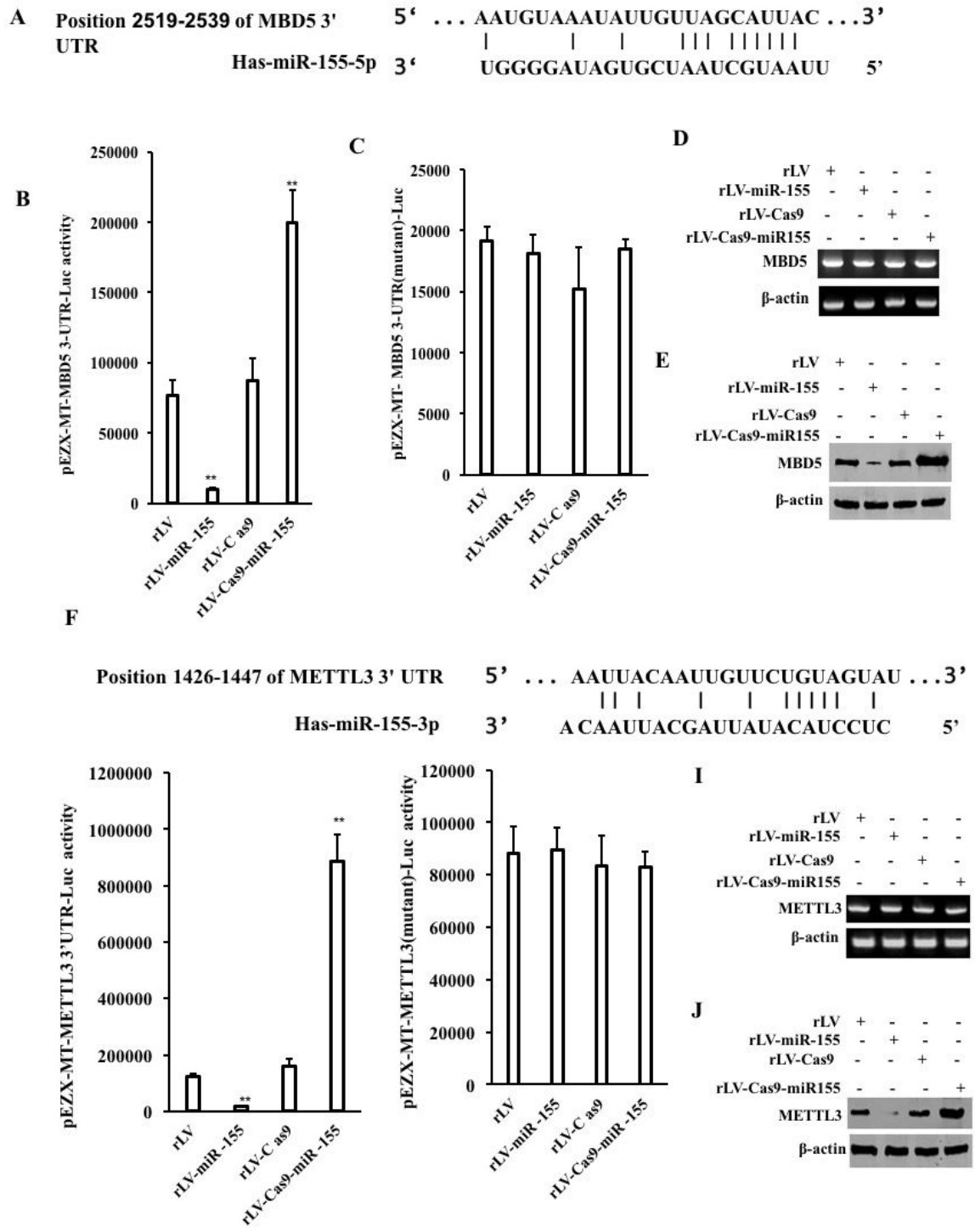

Figure 3

miR-155 targets MBD5 and METTL3 in liver cancer stem cells.A. Using MirTarget scanning soft software, BLAST tools and other bioinformatics methods to analyze the seed sequence of mature miR-155 targeting for MBD5 mRNA 3'-uncoding region (UTR). B. pEZX-MT-MBD5 3'UTR-Luc dual luciferase reporter gene activity was tested. C. pEZX-MT-MBD5 3'UTR (mutant) -Luc dual luciferase reporter gene activity was tested. D. Reverse transcription polymerase chain reaction (RT-PCR) was used to detect the

transcription ability of MBD5, β-actin was used as internal reference gene. E. Western blotting was used to detect the translation ability of MBD5, β-actin was used as the internal reference gene. F. Analyze the seed sequence of mature miR-155 targeting for METTL3 mRNA 3'-uncoding region (UTR) using bioinformatics methods such as MirTarget scanning soft software and BLAST tools. G. pEZX-MT-METTL3 3'UTR-Luc luciferase reporter gene activity for detection H. pEZX-MT-METTL3 3'UTR (mutant) -Luc luciferase reporter gene activity for detection. I. RT-PCR was used to detect the transcription ability of METTL3, and β-actin was used as the internal reference gene. J. Western blotting was used to detect the translation ability of METTL3, and β-actin was used as the internal reference gene.

Figure 4

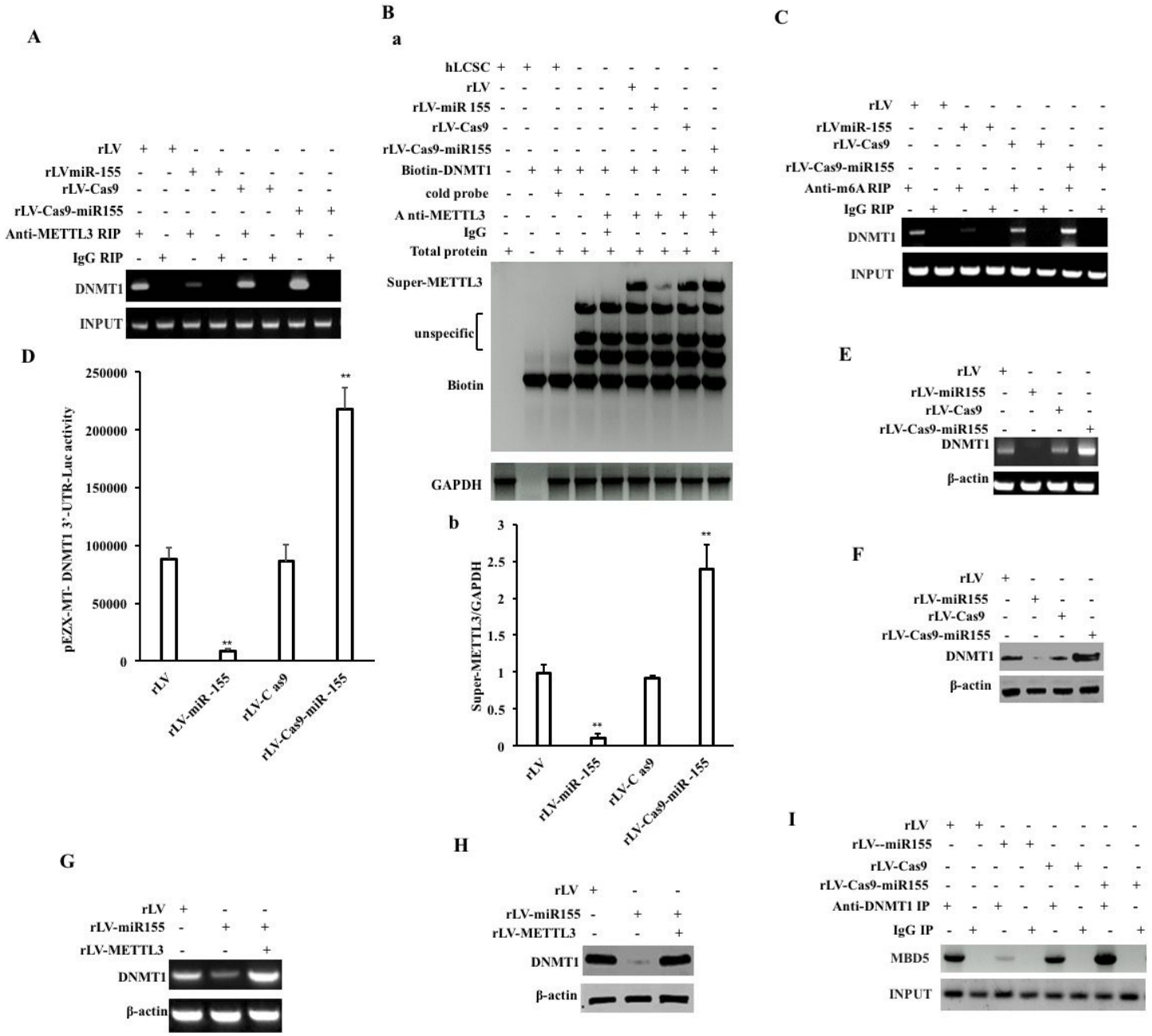

Figure 4

miR-155 reduces the expression DNMT1 and the interaction between MBD5 and DNMT1 in human liver cancer stem cells. A. Anti-METTL3 RNA co-precipitation (RIP) analysis. IgG RNA co-precipitation served as a negative control. B. Using Biotin labeled DNMT1 mRNA probe (Biotin-DNMT1 mRNA) and anti-METTL3, anti-Biotin for Super-RNA-protein complex gel migration experiment (Super-RNA-EMSA), IgG super-RNA-EMSA served as a negative control. C. pEZX-MT-DNMT1 3'UTR-Luc luciferase reporter gene activity was tested. E. RT-PCR to detect the transcriptional ability of DNMT1, β-actin as an internal reference gene. F. Western blotting was used to detect the translation ability of DNMT1, and β-actin was used as an internal reference gene. G. RT-PCR to detect the transcriptional ability of DNMT1, β-actin as an internal reference gene. H. Western blotting was used to detect the translation ability of DNMT1, and β-actin was used as the internal reference gene. I. The co-immunoprecipitation with anti-MBD5 and Western blotting with anti-DNMT1. IgG co-precipitation was used as a negative control. The samples before co-precipitation were subjected to Western blotting with anti-MBD5 as INPUT.

Figure 5

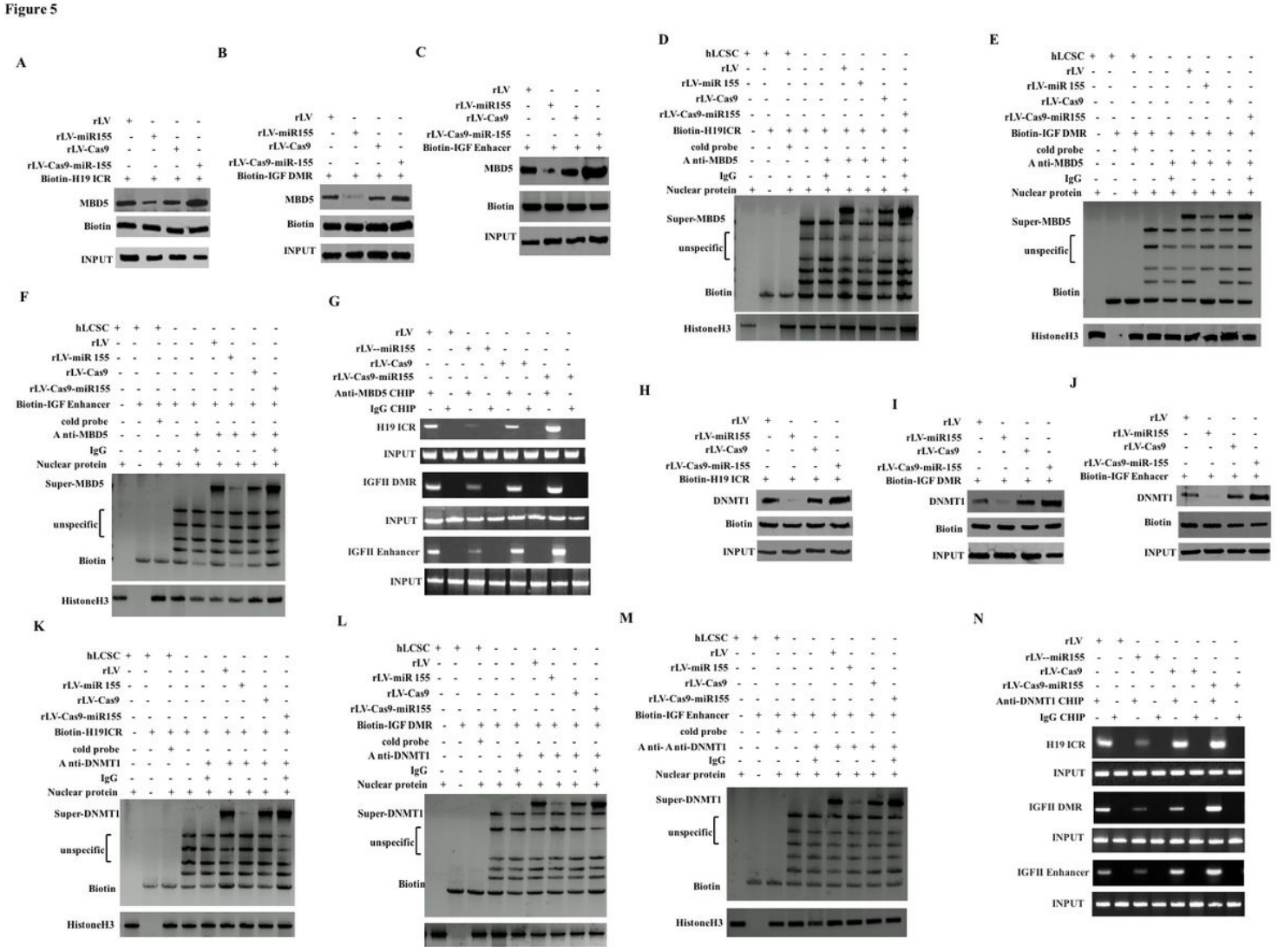

Figure 5

miR155 inhibits the binding of MBD5, DNMT1 to three DNA methylation binding regions (H19 ICR, IGFII DMR, IGFII Enhancer) of IGFII. A. DNA pulldown to analyze the interaction between the probes of three

DNA methylation binding sequences (H19 ICR, IGFII DMR, IGFII Enhancer) and MBD5. B. DNA pulldown method was used to analyze the interaction between the three DNA methylation binding sequences (H19 ICR, IGFII DMR, IGFII Enhancer) probes and MBD5. C. DNA pulldown method to analyze the interaction between the probes of three DNA methylation binding sequences (H19 ICR, IGFII DMR, IGFII Enhancer)and MBD5 a. D. Super-DNA gel migration was used to determine the binding ability of MBD and H19 ICR DNA probe. E. Super-DNA-protein complex gel migration experiment (Super-EMSA) with Biotin labeled IGFII DMR DNA probe , anti-MBD5,and anti-Biotin. F. Super-DNA-protein complex gel migration experiment (Super-EMSA).G. Chromosome immunoprecipitation (CHIP) using anti-MBD5.. H. DNA pulldown method to analyze the interaction between three DNA methylation binding sequences (H19 ICR, IGFII DMR, IGFII Enhancer) probes and DNMT1. I. DNA pulldown method to analyze the interaction between three DNA methylation binding sequences (H19 ICR, IGFII DMR, IGFII Enhancer) probes and DNMT1. J. DNA pulldown method to analyze the interaction between three DNA methylation binding sequences (H19 ICR, IGFII DMR, IGFII Enhancer) probes and DNMT1.K. Super-DNA-protein complex gel migration experiment (Super-EMSA) using biotin labeled H19 ICR DNA probe (Biotin-H19 ICR DNA) , anti-MBD5 and anti-Biotin, using IgG The super-EMSA was used as a negative control, the EMSA without nucleoprotein and the EMSA with excess cold probe added as the system reference, and the hybridization band of Biotin-H19 ICR DNA and the amount of added nucleoprotein were used as INPUT.L. Super-DNA-protein complex gel migration experiment (Super-EMSA) using Biotin-labeled IGFII DMR DNA probe and anti-DNMT1, anti-Biotin. M. Super-DNA-protein complex gel migration experiment. N. Chromosome immunoprecipitation (CHIP) using anti-DNMT1.

Figure6

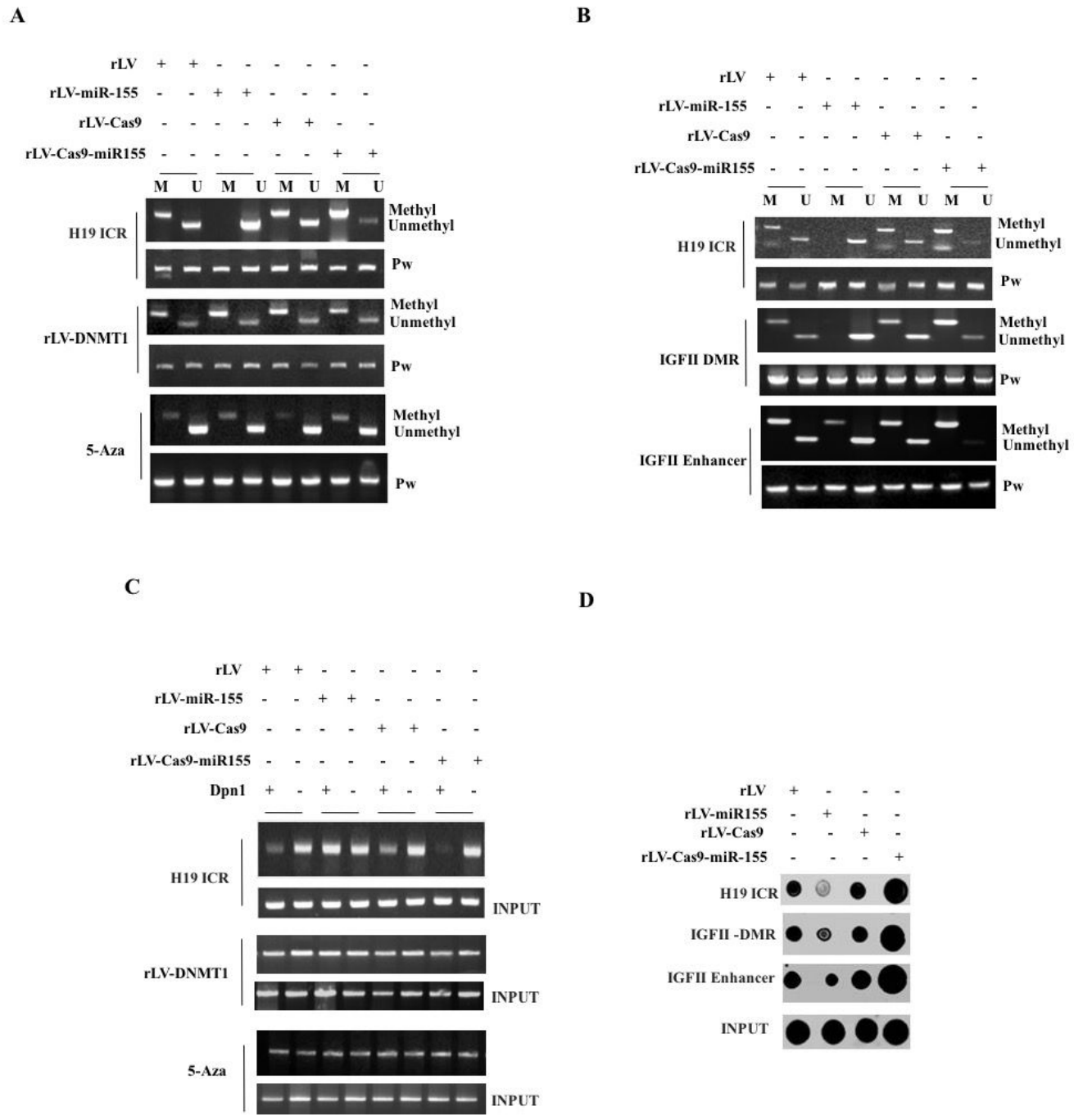

Figure 6

miR155 inhibits methylation modification of three DNA regions on IGFII (H19 ICR, IGFII DMR, IGFII Enhancer). A. The specific methylation PCR to analyze the DNA methylation modification. B. Specific methylation PCR analysis of DNA methylation modification of IGFII DMR and IGFII Enhancer. C. Analysis of DNA methylation modification of H19 ICR, IGFII DMR, IGFII Enhancer by D pnI methylation PCR method. D. Method of specific methylation Dot blot analysis of DNA methylation modification of IGFII DMR and IGFII Enhancer.

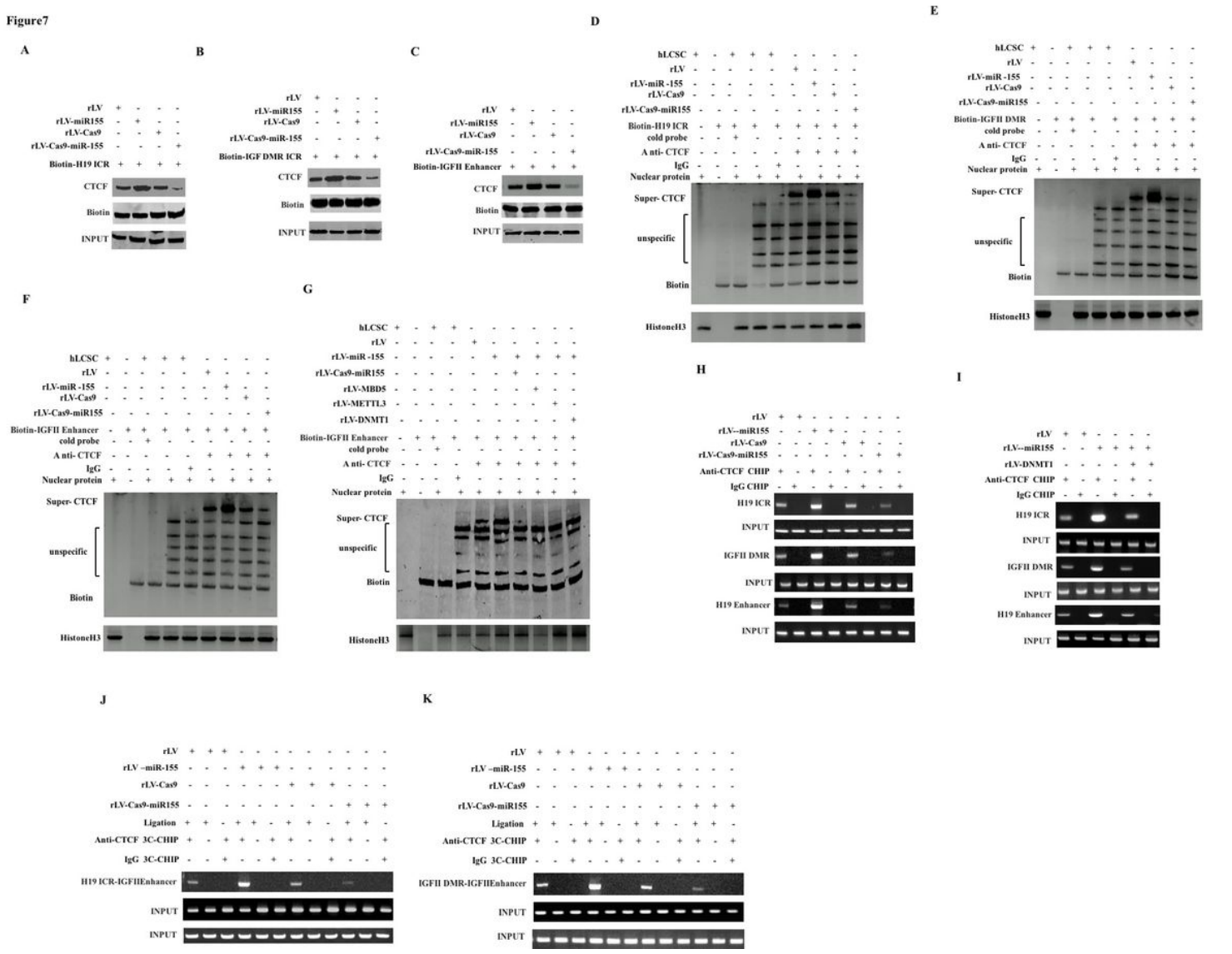

Figure 7

miR-155 enhances the formation of IGFII DNA loops (H19 ICR- IGFII Enhancer, IGFII DMR-IGFII Enhancer) in liver cancer stem cells. A. DNA pulldown to analyze the binding ability of CTCF to IGFII H19 ICR probes. B. DNA pulldown to analyze the binding ability of CTCF to IGFII DMR probes. C. DNA pulldown to analyze the binding ability of CTCF to IGFII Enhancer probes D. Super-DNA gel migration was used to determine the binding ability of CTCF and H19 ICR DNA probe. The biotin labeled H19 ICR DNA probe, anti-CTCF, anti-Biotin for Super-EMSA. E. Super-DNA gel migration was used to determine the binding ability of CTCF and IGFII DMR DNA probe. F. Super-DNA gel migration was used to determine the binding ability of CTCF and IGFII Enhancer DNA probe. G. Super-DNA gel migration migration was used to determine the binding ability of CTCF to H19 ICR DNA probe. H. Chromosome immunoprecipitation (CHIP) using anti-CTCF. The DNA isolated and purified from CHIP precipitate was used as the template, according to H19 ICR, IGFII DMR, The primers designed by IGFII Enhancer DNA sequence were amplified by polymerase chain reaction (PCR). IgG CHIP was used as a negative control; using the DNA retained before chromatin immunoprecipitation as a template, and the product amplified with primers designed by H19 ICR, IGFII

DMR, and IGFII Enhancer DNA sequences as an internal reference (INPUT). I. Chromosome immunoprecipitation (CHIP) using anti-CTCF. J. Analysis of the binding capacity of CTCF and H9 ICR-IGFII Enhancer by chromosomal configuration capture (3C) -chromatin immunoprecipitation (CHIP) method. The cells were cross-linked with formaldehyde and then chromosomal configuration capture (3C) -chromatin immunoprecipitation (CHIP) with anti-CTCF. Using the DNA isolated and purified from the CHIP-3C precipitate as a template, polymerase chain reaction (PCR) amplification was performed using a pair of mixed primers designed according to H9 ICR and IGFII Enhancer. IgG CHIP-3C was used as a negative control; the DNA retained before chromatin immunoprecipitation was used as a template, and the products amplified by independent primers designed by H9 ICR and IGFII Enhancer were used as internal reference (INPUT). K. The binding ability of CTCF and IGFII DMR-IGFII Enhancer in cells by chromosomal configuration capture (3C) -chromatin immunoprecipitation (CHIP).

Figure 8

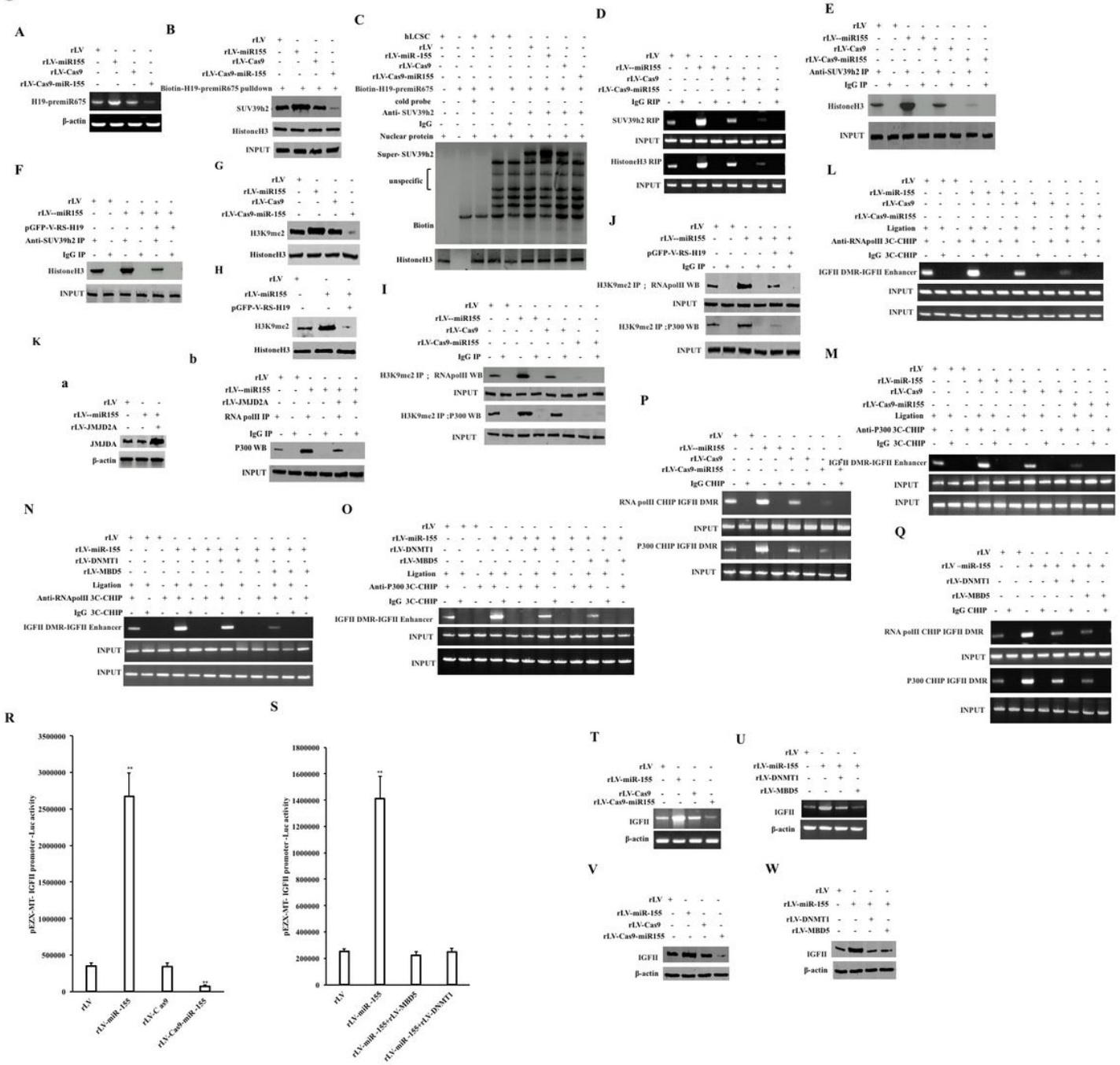

Figure 8

miR155 promotes the expression analysis of IGFII through IGFII DNA loop A. RT-PCRwas used to detect the transcription ability of H19-pre miR675.β-actin was used as the internal reference gene. B. RNA pulldown method to analyze the binding ability of H19-pre miR675 probe to histone methyltransferase SUV39h2. C. Super-RNA gel migration was used to determine the binding ability of H19-pre miR675 probe and histone methyltransferase SUV39h2. D. RNA immuncoprecipitation (RIP) with Anti-SUV39h2 or anti-Histone H3. Using the RNA isolated and purified from the RNA co-precipitate as a template, the primers designed by the H19-pre miR675 sequence were used to amplify DNMT1. IgG RIP was used as a negative control.. E. Co-immunoprecipitation with anti-SUV39h2 F. Co-immunoprecipitation with anti-SUV39h2. G. Western blotting was used to detect the H3K9me2, and HistoneH3 was used as the internal reference gene. H. Western blotting was used to detect the H3K9me2 ,and HistoneH3 was used as the internal reference gene. I. Co-immunoprecipitation with anti-H3K9me2. J. Co-immunoprecipitate with anti-H3K9me2. K. a. Western blotting analysis using anti-JMJD2A. β-actin as an internal reference gene. b. Co-immunoprecipitation with anti-H3K9me2. L. Chromosome configuration capture (3C) -chromatin immunoprecipitation (CHIP) was used to analyze the ability of RNA PolII to enter the IGFII DMR-IGFII Enhancer loop. M. Chromosome configuration capture (3C) -chromatin immunoprecipitation (CHIP) with anti-RNApolII. N. Analysis of the ability of RNA PolII into the IGFII DMR-IGFII Enhancer loop by chromosomal configuration capture (3C) -chromatin immunoprecipitation (CHIP). O. Chromosome configuration capture (3C) -chromatin immunoprecipitation (CHIP) with anti-RNApolII. P. Chromosome immunoprecipitation (CHIP) using anti-RNApolII and P300. Q. Chromosome immunoprecipitation (CHIP) using anti-RNApolII and P300. R. pEZX-MT-IGFII promoter-Luc luciferase reporter gene activity was detected. S. pEZX-MT-IGFII promoter-Luc luciferase reporter gene activity was detected . T. RT-PCR to detect the transcription ability of IGFII . β-actin as an internal reference gene. U. RT-PCR to detect the transcription ability of IGFII .β-actin as the internal reference gene V. Western blotting to detect IGFII .β-actin as an internal reference gene. W. Western blotting was used to detect the IGFII .β-actin was used as the internal reference gene.

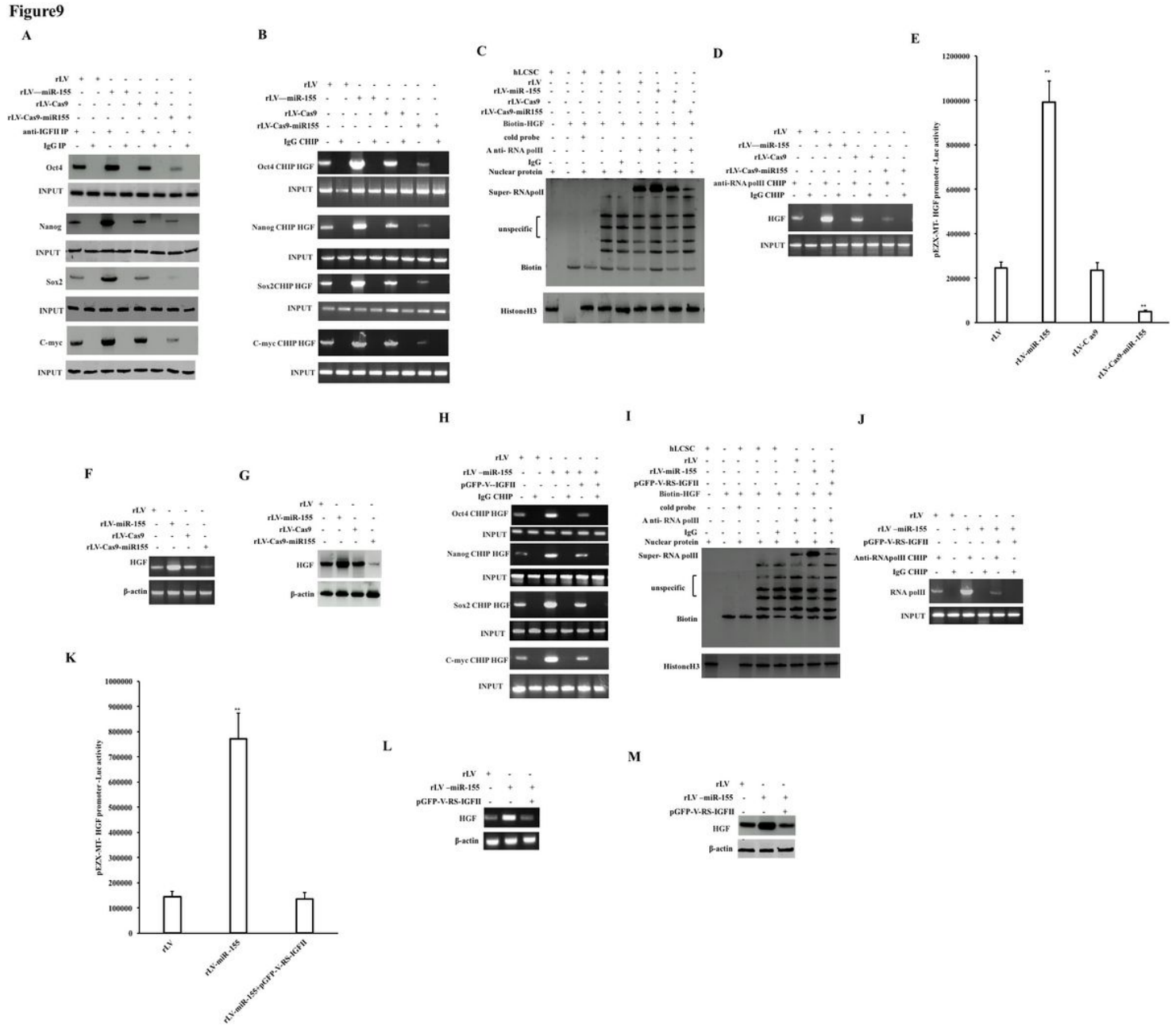

Figure 9

miR-155 enhances the expression of HGF dependent on IGFII t in human liver cancer stem cells A. Co-immunoprecipitation with anti-IGFII and Western blotting with anti-Oct4, anti-Nanog, anti-Sox2, and anti-C-myc. IgG IP was used as a negative control.B. Chromosome immunoprecipitation (CHIP) using anti-Oct4, anti-Nanog, anti-Sox2, and anti-C-myc. C. Super-DNA-protein complex gel migration (Super-EMSA) using Biotin labeled HGF promoter probe (Biotin-HGF promoter) , anti-RNApolII, and anti-Biotin for. D. Chromosome immunoprecipitation (CHIP) using anti-RNApolII. E. pEZX-MT-HGF promoter-Luc luciferase reporter gene activity. Each experiment was repeated three times. The values of each group are expressed as mean ± standard deviation (mean ± SEM, n = 3), **, P <0.01, *, P <0.05. F. RT-PCR was used to detect the transcription ability of HGF, and β-actin was used as an internal reference gene. G. Western blotting to detect the translation ability of HGF. β-actin as the internal reference gene. H. Chromosome

immunoprecipitation (CHIP) using anti-Oct4, anti-Nanog, anti-Sox2, and anti-C-myc. I. Super-DNA-protein complex gel migration experiment (Super-EMSA). J. Chromosome immunoprecipitation (CHIP) using anti-RNApolII. K. The assay of pEZX-MT-HGF promoter-Luc luciferase reporter gene activity. L. RT-PCR was used to detect the transcription ability of HGF. β-actin was used as an internal reference gene. M. Western blotting was used to detect the translation ability of HGF . β-actin was used as the internal reference gene.

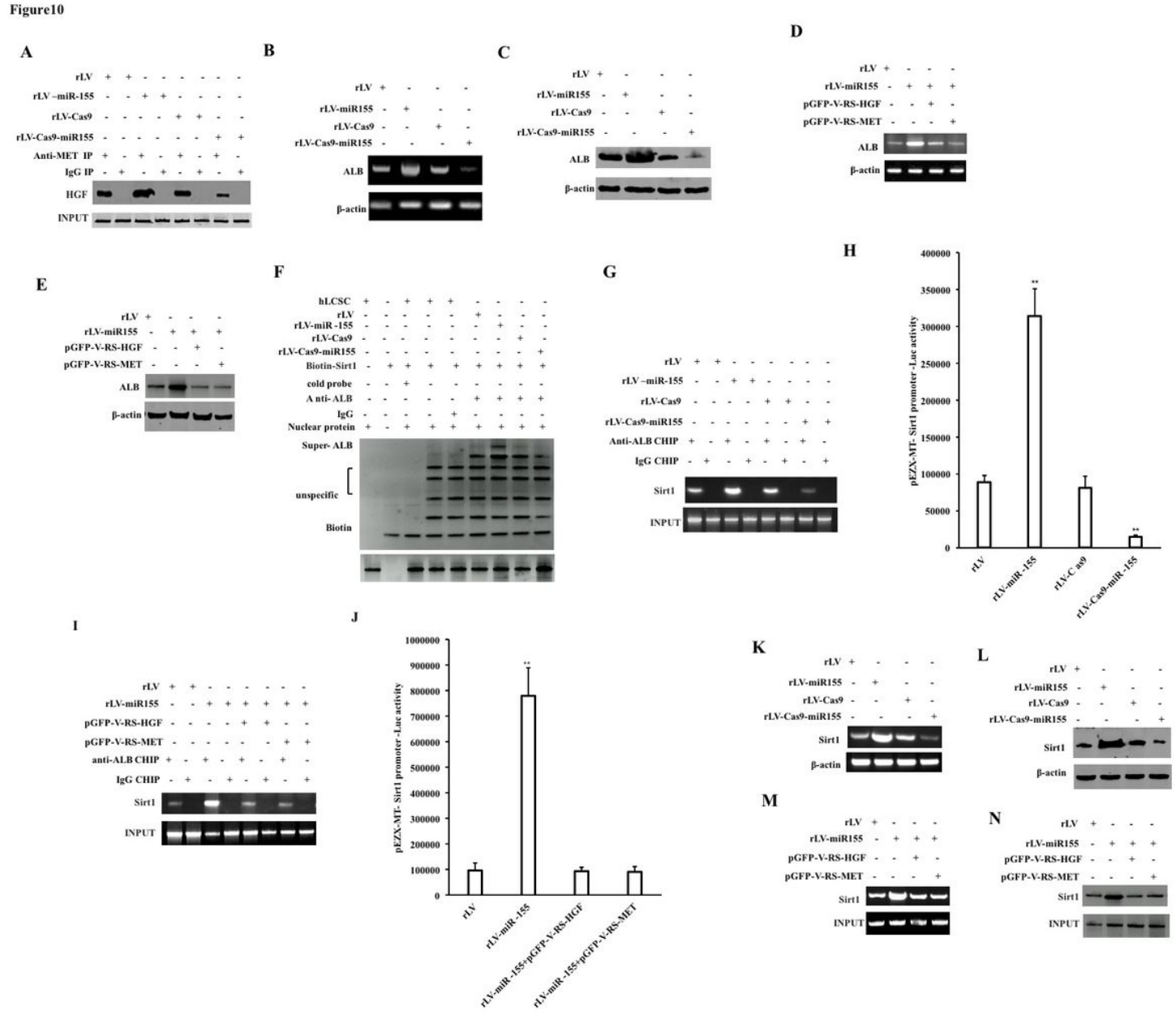

Figure 10

miR155 promotes Sirt1 expression dependent on HGF-c-MET in human liver cancer stem cells. A. Co-immunoprecipitation with anti-HGF and the precipitates were analyzed by Western blotting with anti-c-MET. B. RT-PCR to detect the transcriptional capacity of ALB in cells.β-actin as an internal reference gene.C. Western blotting was used to detect the translation ability of ALB . β-actin was used as the internal reference gene. D. RT-PCR was used to detect the transcription ability of ALB . β-actin was used

as an internal reference gene. E. Western blotting was used to detect the translation ability of ALB . β-actin was used as the internal reference gene. F. Super-DNA-protein complex gel migration experiment (Super-EMSA) Using Biotin-labeled Sirt1 promoter probe ,and anti-ALB, and anti-Biotin. G. Chromosome immunoprecipitation (CHIP) using anti-ALB. H. Detection of pEZX-MT-Sirt1 promoter-Luc luciferase reporter gene activity. I. Chromosome immunoprecipitation (CHIP) using anti-ALB. J. The activity of pEZX-MT-Sirt1 promoter-Luc dual luciferase reporter gene. K. RT-PCR to detect the transcriptional ability of Sirt1 .β-actin as an internal reference gene. L. Western blotting was used to detect the translation ability of Sirt1 . β-actin was used as an internal reference gene. M. RT-PCR was used to detect the transcriptional ability of Sirt1. β-actin was used as an internal reference gene. N. Western blotting was used to detect the translation ability of Sirt1 i. β-actin is used as an internal reference gene.

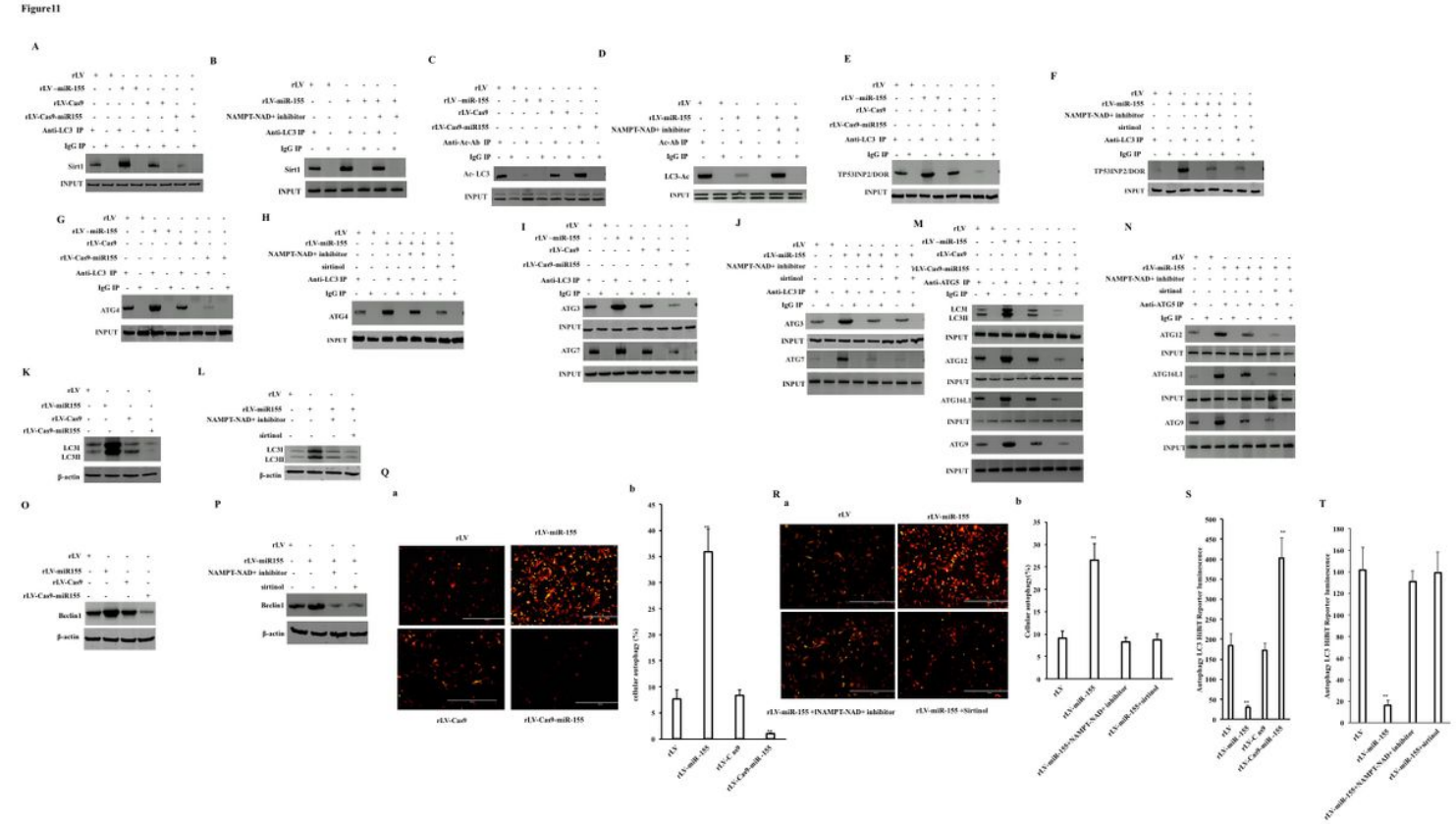

Figure 11

miR-155 enhances the occurrence of autophagy through Sirt1 to in liver cancer stem cells. A. The Co-immunoprecipitation with anti-LC3 and Western blotting with anti-Sirt1. IgG co-immunoprecipitation was used as a negative control. B. Co-immunoprecipitation with anti-LC3 and Western blotting with anti-Sirt1. C. Co-immunoprecipitation with anti-Ac-Ab and Western blotting with anti-LC3. D. Co-immunoprecipitation with anti-Ac-Ab and Western blotting with anti-LC3. E. Co-immunoprecipitation with anti-LC3 andWestern blotting anti-TP53INP2 / DOR. F. Co-immunoprecipitation with anti-LC3 andWestern blotting anti-TP53INP2 / DOR. G. Co-immunoprecipitation t with anti-LC3 and Western blotting with anti-ATG4. H. Co-immunoprecipitation with anti-LC3 and Western blotting with anti-ATG4. I. Co-immunoprecipitation with anti-LC3 and Western blotting with anti-ATG3 and anti-ATG7. J. Co-immunoprecipitation with anti-LC3 and Western blotting with anti-ATG3 and anti-ATG7. K. Western blotting was used to detect the levels of

LC3I / II . β-actin was used as the internal reference gene. L. Western blotting was used to detect the levels of LC3I / II . β-actin was used as the internal reference gene. M. Co-immunoprecipitation with anti-ATG5 and Western blotting with anti-ATG12 and anti-ATG16L1 anti-ATG9. N. Co-immunoprecipitation with anti-ATG5 and Western blotting with anti-ATG12 and anti-ATG16L1 anti-ATG9. O. Western blotting was used to detect the expression of beclin1.β-actin was used as the internal reference gene. P. Western blotting was used to detect the expression of beclin1.β-actin was used as the internal reference gene. Q. a. Cell autophagy Monitoring using the rAd-Cherry-GFP-LC3 through the fluorescence microscope (Red marker Cherry-LC3). b. Comparison of the incidence of cell autophagy. Each experiment was repeated three times. The values of each group are expressed as mean ± standard deviation (mean ± SEM, n = 3), **, P <0.01, *, P <0.05. R. a. Cell autophagy Monitoring using the rAd-Cherry-GFP-LC3 through the fluorescence microscope (Red marker Cherry-LC3). b. Comparison of the incidence of cell autophagy. S-T. autophagy-LC3-inhibit-reporter assay (LC3 HiBiT Reporter Assay System) .

Figure12

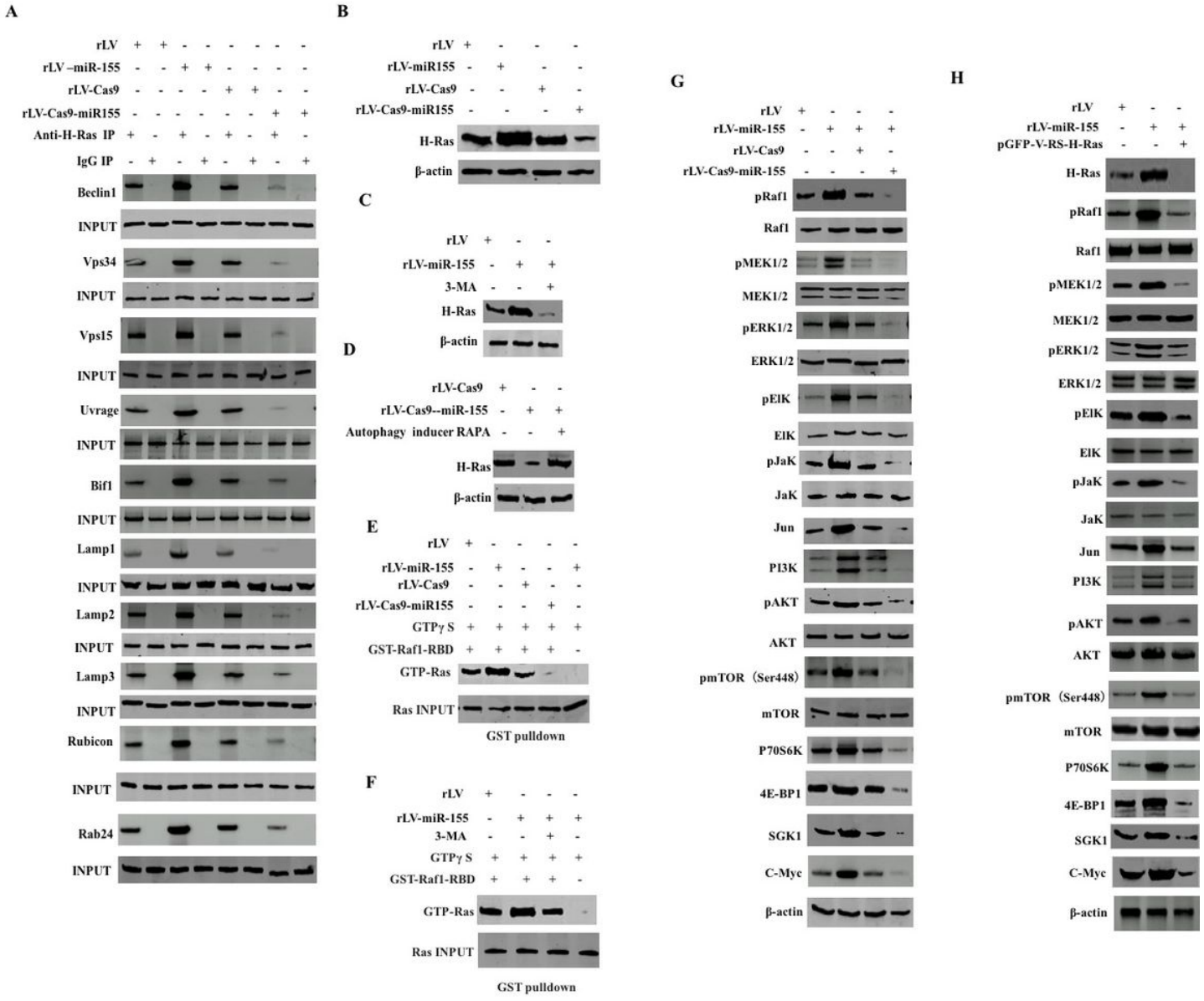

Figure 12

miR155 enhances the expression levels of pRaf1, pMEK1 / 2, pERK1 / 2, pElK, pJak, Jun, pAKT, pmTOR, P70S6K, 4E-BP1, SGK1, C-myc dependent on H-Ras in human human liver cancer stem cells. A. Co-immunoprecipitation with anti-H-Ras and Western blotting with anti-ATG3, anti-Beclin1, anti-Vps34, anti-Vps5, anti-Uvrage, anti-Bif1, anti-Lamp1, -Lamp2, anti-lamp3, anti-rubicon, anti-Rab24. B. Western blotting was used to detect the translation ability of H-Ras .β-actin was used as the internal reference gene. C. Western blotting was used to detect the translation ability of H-Ras.β-actin was used as the internal reference gene. D. Western blotting was used to detect the translation ability of H-Ras .β-actin was used as the internal reference gene. E. GST pulldown analysis with anti-GST. The precipitate was analyzed by Western blotting with anti-GTP-Ras. F. GST pulldown analysis with anti-GST. The precipitate was analyzed by Western blotting with anti-GTP-Ras. G&H. Western blotting to detect pRaf1, pMEK1 / 2, pERK1 / 2, pElK, pJak, Jun, pAKT, pmTOR, P70S6K, 4E-BP1, SGK1, C-myc .β-actin as an internal reference gene.

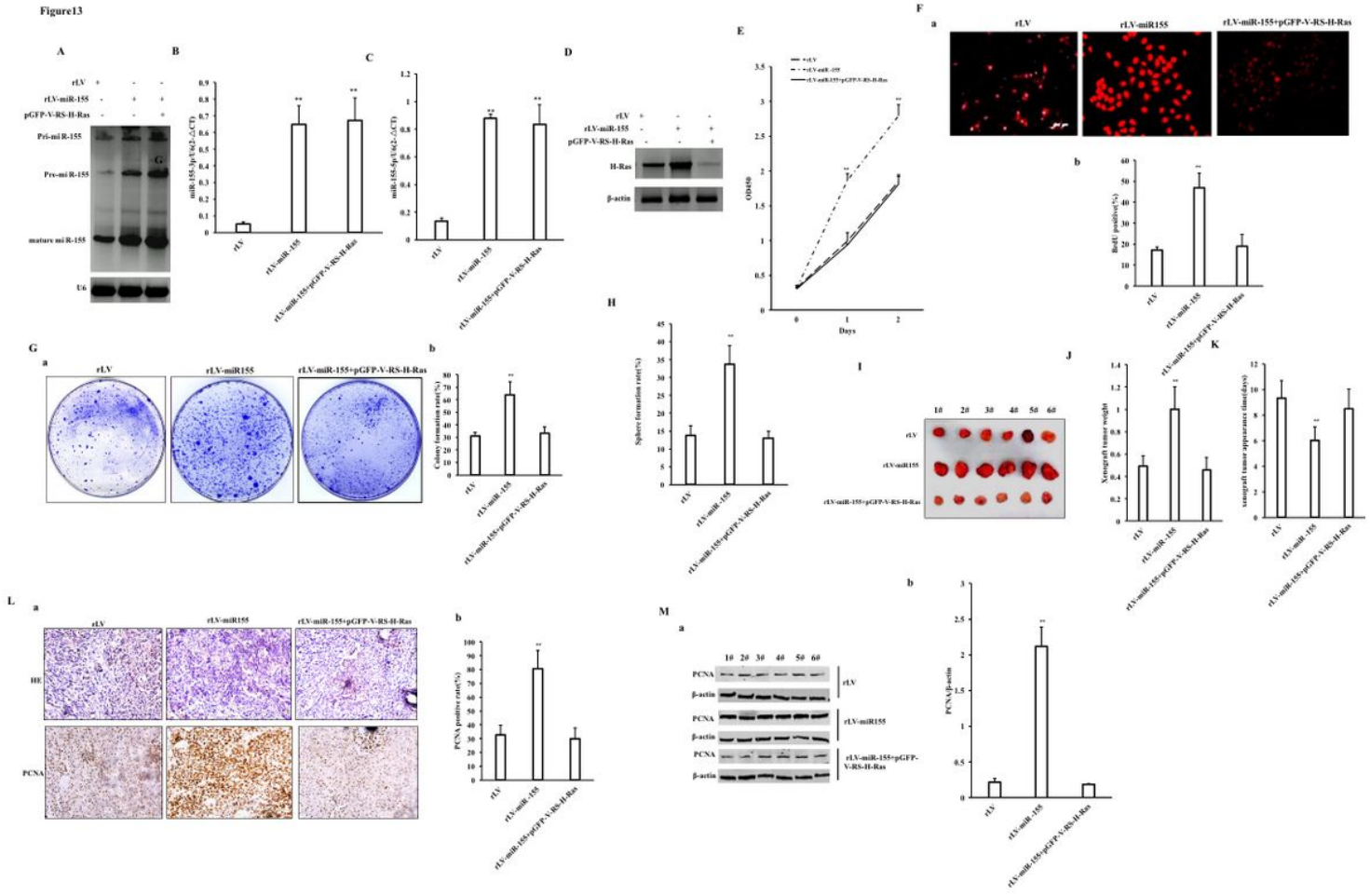

Figure 13

-Ras knockdown abolished the oncogenic function of miR-155 in liver cancer stem cells.A. Northern blotting for miR-155 . U6 is used as an internal reference gene. B. Real-time RT-PCR for mature miR-15-3p. U6 as an internal reference gene. C. Real-time RT-PCR for mature miR-15-5p. U6 as an internal reference

gene. D. Western blotting was used to detect the expression of H-Ras.β-actin as an internal reference gene. E. The cell proliferation ability was measured by CCK8 method. F. BrdU staining analysis . a. BrdU staining photo. 2. BrdU positive rate. G. plate colony formation ability. A. Photograph of plate colonies b. colony formation rate.H. The sphere formation ability. I. Cells were inoculated into the axillary skin of Balb / C nude mice for one month and Photographagy of The transplanted tumor (xenograft). J. Comparison of the size (g) of transplanted tumors. K. Comparison of appearance time (days) of transplanted tumors. L. a.4% formaldehyde-fixed, paraffin-embedded transplanted tumor tissue sections (4 μm) were stained with hematoxylin-eosin (HE) (original magnification × 100) and performed immunostaining of proliferating cell nuclear antigen (PCNA). b. PCNA positive rate.M. a&b Western blotting to detect the expression of PCNA β-actin as an internal reference gene.

Figure14

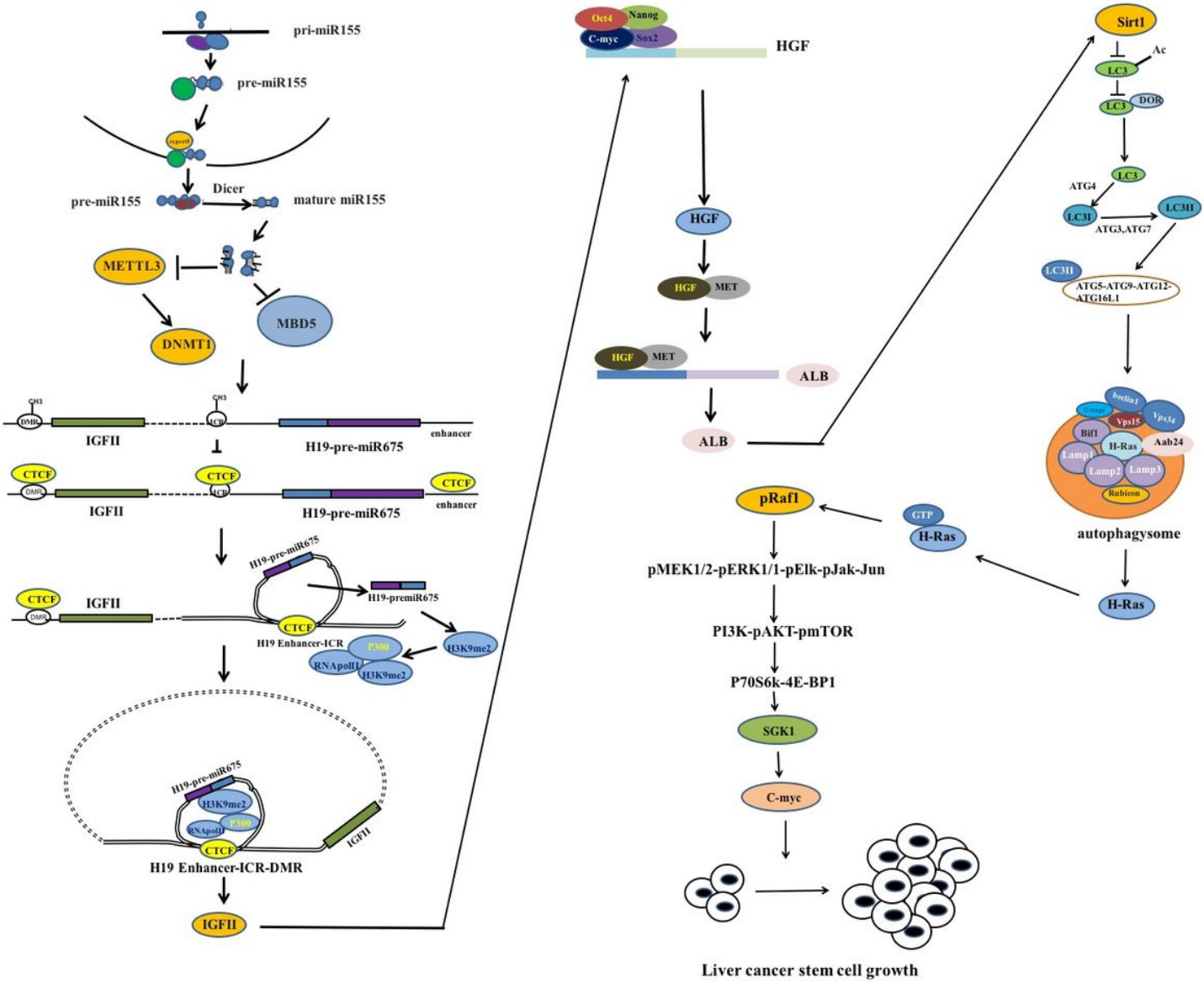

Figure 14

Schematic diagram of the effective mechanism of miR-155 in the progression of liver cancer stem cells.

Supplementary Files

This is a list of supplementary files associated with this preprint. Click to download.

- supplementalData.docx